Amyotrophic Lateral Sclerosis Proteomic Signature And Treatment With Mesenchymal Stem Cell-derived Extracellular Vesicles

Suzy Varderidou-Minasian[1], Svetlana Pasteuning-Vuhman[2], Annabel Timmers[1], Maarten Altelaar[3,4], Magdalena J Lorenowicz[5,6], R Jeroen Pasterkamp[1].

[1] Department of Translational Neuroscience, UMC Utrecht Brain Center, University Medical Center Utrecht, Utrecht University, 3584 CG Utrecht, The Netherlands.
[2] VectorY. Matrix Innovation Center, Science Park 408, 1098 XH Amsterdam
[3] Biomolecular Mass Spectrometry and Proteomics, Bijvoet Center for Biomolecular Research and Utrecht Institute for Pharmaceutical Sciences, University of Utrecht, Padualaan 8, 3584 CH Utrecht, The Netherlands.
[4] Netherlands Proteomics Center, Padualaan 8, 3584 CH Utrecht, The Netherlands.
[5] Center for Molecular Medicine, University Medical Center Utrecht, Universiteitsweg 100, 3584 CG, Utrecht, The Netherlands.
[6] Regenerative Medicine Center, Uppsalalaan 8, 3584 CT, Utrecht, The Netherlands.

Keywords: Amyotrophic Lateral Sclerosis, induced pluripotent stem cells, Mesenchymal stem/stromal cells; extracellular vesicles; mass spectrometry; proteomics

Correspondence:

Suzy Varderidou-Minasian, PhD
Address: Utrecht University, 3584 CG Utrecht, The Netherlands
Email: S.varderidou-3@umcutrecht.nl

Abstract

Amyotrophic lateral sclerosis (ALS) is a progressive neurodegenerative disorder with a lifetime risk of 1:400, primarily affecting upper and lower motor neurons. Unfortunately, there are only two drugs approved to treat ALS, which increase patient survival only by a few months. This highlights the urgent need for developments of new ALS modifying therapies, which have been hampered by high failure rate of new drug candidates during clinical trials.

Stem cell therapy is one of the promising approaches that is in development for treating ALS. The beneficial effects of stem cell therapy rely on their paracrine signaling, suggesting extracellular vesicles (EVs) as possible non-cell based therapy. In particular, mesenchymal stem cells (MSCs) contribute to reparative process.

To better translate and assess therapeutic potential of MSC-EVs, we combined state of the art induced pluripotent stem cell (iPSC) technologies to obtain patient-derived spinal low motor neurons and a comprehensive proteomic analysis to decipher the proteomic signature.

To investigate the key molecular perturbations underlying disease pathology of ALS, a comprehensive proteomic analysis was performed showing mutation-specific and common ALS-specific changes. Mutation-specific effects in ALS motor neurons with hexanucleotide expansion in C9ORF72 exhibit dysregulation in *proteins targeting to ER* and *cytoplasmic translation*. In FUS-ALS motor neurons, *iron ion homeostasis* and *cellular response to stress* processes are affected. In ALS-TDP-43 motor neurons *protein transport* and *localization* are affected. Common ALS mechanisms such as *mRNA splicing, proteasomal ubiquitin* and *mitochondrial associated processes* are dysregulated.

Furthermore, we demonstrated these underlying dysregulated mechanisms after treatment with MSC-EVs. More importantly, MSC-EV treatment can restore the protein expression levels impaired in ALS suggesting for future therapeutic potential for ALS.

Introduction

Amyotrophic lateral sclerosis (ALS) is an adult-onset neurodegenerative disease characterized by progressive muscle weakness and loss of upper and lower motor neurons in the brain and spinal cord [1, 2]. Patients eventually die of respiratory failure 2-4 years after onset [3]. The incidence of ALS is between 1.5 and 2 individuals per 100,000 per year [4] with an average age of onset between 58-60 years. ALS arises from a combination of genetic and environmental factors. Classically, 5-15% of the cases have a family history (defined as familial ALS; fALS), whereas 85-95% of the cases lack a hereditary cause (defined as sporadic ALS; sALS) [5]. More than 40 different genes have been linked to familial form of ALS [6] with mutations mainly in one of the following genes: -Chromosome 9 open reading frame 72 (*C9ORF72*; ~40%) [7, 8], -Superoxide dismutase 1 (*SOD1*; ~20%) [9], -Fused in sarcoma (*FUS*; ~1-5%) [10], and -TAR DNA binding protein 43 (*TDP-43*; ~1-5%) [11]. Main pathological mechanisms underlying ALS include

a dysfunction in RNA metabolism and protein homeostasis. More specifically, defects in nucleocytoplasmic trafficking, accumulation of toxic aggregates and their prion-like spread from cell-to-cells leading to selective degeneration of motor neurons due to ROS, mitochondrial defects and neuromuscular junction dysfunction [12, 13]. Despite the extraordinary recent progress in understanding the biology of ALS, meaningful therapies for ALS are still lacking. Drugs currently used to treat ALS are *Riluzole* and *Edaravone* which are approved by the United States Food and Drug Administration [14]. They prolong the survival in ALS with few months or slow down functional decline. There is no curative treatment for ALS, therefore development of new, effective therapies are needed.

In the last decade, stem cell therapy has been attempted as promising therapeutic approach for ALS [15]. In particular, mesenchymal stem cells (MSCs) are of great interest due to their easy availability, ability to migrate to damaged tissue and contribute to reparative process [16-18]. MSCs delay motor neuron death, decrease inflammatory response and prolong survival [19, 20]. In the last years, several clinical trials injected MSCs in ALS patients showing feasibility, safety and immunological effects [21]. However, evidence indicates that the beneficial effects of stem cell therapy rely on their paracrine signaling rather than their engraftment, shifting the focus from cells to their secretome [22]. In particular, some evidence indicate that the secretome can exert similar therapeutic potential as their cells of origin [23-25]. Moreover, stem cells cannot cross the blood-brain barrier (BBB), so especially in neurodegenerative disorders, the beneficial effects rely on the secretome [22].

Extracellular vesicles (EVs) are heterogeneous group of membrane vesicles released from various cells. According to their origin and size, they can be classified into three main subtypes: -exosomes (40-140 nm) are formed from the endosomal origin [26]. – microvesicles (50-1000 nm) bud directly off the plasma membrane [27], and – apoptotic bodies (1-5 µm) are released when cells undergo apoptosis [28]. Due to lack of reliable tools and specific markers to distinguish EV subtypes, we will refer exosomes and microvesicles as EVs [29]. EVs act as intracellular shuttle transporting cargo such as proteins, RNA, lipids and carbohydrates between cells. The specific cargo composition depends on the tissue/cell of origin [30, 31]. The application of MSC-EVs as cell-free therapy is due to their small size, which lowers risk of vascular obstructions and allows crossing the BBB. Moreover, injection of EVs also carries a lower safety risk, as they cannot self-replicate. MSC-EVs contain molecules having a major role in the regulation of development, differentiation and cell survival [32, 33]. MSC-EVs selectively promoted neurite outgrowth in cortical neuron cultures, and regulate neural plasticity, which can be a valuable treatment for ALS [34, 35].

To get insight into the mechanisms underlying ALS and to enable testing new therapeutic agents, we applied a state-of-the-art human induced pluripotent stem cells (hiPSC) with high-throughput mass spectrometry (MS) approach to explore in-depth characterization of involved pathways. MS-based proteomic methods are being increasingly applied to better understand disease-related mechanisms [36, 37]. Proteins are the functional

components that drive the majority of cellular processes. In this study, we characterized the proteins involved in several ALS-related mutations and evaluated the beneficial effect and the proteome changes after MSC-EV treatment.

Spinal lower motor neurons were derived from iPSC lines carrying mutations in C9ORF72 (Hexanucleotide repeat expansion (6-8kb)), FUS (R495QfsX527) or TDP-43 (I383T) paired with their controls from the same subject. We identified unique proteomic signatures for each ALS mutation (C9ORF72, FUS and TDP-43), as well as universal signatures of ALS. More importantly, the proteomic signature after MSC-EV treatment were associated with recovery in mutation specific and general ALS conditions, suggesting a potential therapeutic approach for ALS.

Results

Generation of iPSC-derived spinal lower motor neurons

The iPSC lines were reprogrammed, characterized, as described elsewhere [38]. The details about the iPSC lines are described in **Table 1**. To generate spinal lower motor neurons, we followed a previously published protocol with some modification [39]. This differentiation protocol produced populations of HB9 and ISL1 positive motor neurons within 25 days (**Figure 1A-D**). Moreover, motor neurons derived from this protocol showed abundant CHAT and SMI32/NFH expression. To further characterize the iPSC-derived motor neurons, we performed gene expression analysis at different stages of differentiation. The differentiated motor neurons showed reduced expression of neuronal stem cell markers *NANOG*, *SOX2*, and *PAX6*, and increased expression of mature motor neuronal markers *ISL1*,*HB9 CHAT*, *NFH*, and *SLC18A3*, encoding the vesicular acetylcholine transporter (VACHT) protein (**Figure 1E**).

ALS mutation specific changes in the proteome

To resolve the proteome changes caused by the mutations in C9ORF72, FUS or TDP-43, we performed high-resolution tandem mass spectrometry (LC-MS/MS) analysis for three biological replicates for each mutation and their CTRLs (**Figure 2A**). We identified up to 6163 proteins with a false discovery rate of 1%. Next, the motor neuron samples were normalized to the reference protein Calnexin, which is a chaperon protein identified in all neuronal samples. The data between samples and replicates was normally distributed (**Figure S1**). A principal component analysis (PCA) of all samples (**Figure 2B**) was performed that provided a general overview of the whole proteome distribution across all the samples. This PCA analysis revealed a clustering between samples from the same line rather that disease versus control. The mutation-specific proteomic signatures were identified within each ALS mutation, where the mutations in C9ORF72, FUS and TDP-43 versus their CTRLs were compared separately (**Figure 2C,**). We considered proteins with a p-value ≤ 0.1 and a fold change ≥ 1.5 as significantly and differentially regulated. This mutation-specific analysis resulted in 17 upregulated and 238 downregulated proteins in C9ORF72, 96 upregulated and 49 downregulated proteins in FUS and 107 upregulated and 57 downregulated proteins in TDP-43 (**Table S1**). In

Figure 2D we highlighted the top 10 most up- and downregulated proteins for each mutation and their expression levels in other two mutations. In C9ORF72 for example, these proteins are involved in membrane fusion, filopodium assembly and metabolic processes. In FUS, the top 10 most dysregulated proteins are involved in autophagy, amino acid starvation and vasculature development. TDP-43 exhibited dysregulated proteins involved in cytoskeleton transport and synaptic vesicle recycling. PPP1R2 (protein phosphatase inhibitor) and HK1 (hexokinase) were differentially expressed in C9ORF72 but remained unchanged in FUS and TDP-43 mutants. To be noted, PPP1R2 was previously described to be altered in a large-scale blood gene expression study in ALS [40]. In addition, HK1 is associated with mitochondrial dysfunction and plays a key role in the bioenergetics metabolism of the motor neurons, which was previously described in SOD1 rats [41]. RHOB (Ras Homolog Family Member B) was highly upregulated in all three mutations C9ORF72, FUS as well as in TDP-43, and was previously described in SOD1 mice [42]. A Gene Ontology (GO) enrichment analysis with respect to biological function and KEGG pathways was conducted to better elucidate biological processes and pathways involved in ALS for each mutation (**Figure S2 and Figure S3**). For C9ORF72, GO analysis identified several biological processed such as glycogen metabolic process and axon choice point recognition being upregulated and protein targeting to membrane and ER being downregulated. KEGG pathways analysis for C9ORF72 revealed autophagy being upregulated and ribosome pathway being downregulated. In FUS, biological processes in translation and macromolecule biosynthetic process were upregulated while mRNA splicing was downregulated. In addition, pathways related to synaptic vesicle cycle were upregulated and spliceosome related pathways were downregulated. In TDP-43, GO terms related to antigen processing and actin filament depolymerization were upregulated while mRNA splicing and mitochondrial respiratory chain complex assembly were downregulated. KEGG pathway analysis revealed neurodegeneration pathways being upregulated and endocytosis and spliceosome being downregulated.

ALS general alterations

After looking at unique proteome signatures for each ALS mutation, we identified common ALS signatures. All ALS mutations in C9ORF72, FUS and TDP-43 were grouped and compared to the grouped controls. Proteins were considered as significantly regulated with a p value ≤ 0.1 and a fold change ≥ 1.5. This analysis resulted in 90 downregulated and 98 upregulated proteins in C9ORF72, FUS and TDP-43 (**Figure 3A, Table S2**). GO analysis revealed biological processes such as protein catabolic processes, cytoskeleton organization and membrane assembly being upregulated. Mitochondrial transport, mRNA splicing and spliceosome were downregulated, which was previously identified on the mutation-specific levels (**Figure 3B**). Furthermore, KEGG pathway analysis identified pathways in metabolism, Alzheimer, ALS and neurodegeneration being affected (**Table S3**). Next, the top 10 most up- and downregulated proteins are highlighted having a role in cellular response to radiation, Wnt signaling and in actin filament organization (**Figure 3C**). In **Figure 4A** we summarized the dysregulated processes specific for each ALS

mutation, shared between mutations as well as common dysregulated processes in ALS. Since many cellular processes have been identified as potentially contributing to disease progression, we zoomed into several of these processes highlighting the protein expression levels. For example, formation of stress granules in response to cellular stress is a well-recognized pathogenic mechanism in ALS, and here specifically dysregulated in FUS (**Figure 4B**). Proteins targeting to ER are specifically dysregulated in C9ORF72 (ribosomal proteins), and several groups show that ribosomal proteins are key constituents of the toxic DPR proteins [43, 44]. Interestingly, mitochondrial electron transport is dysregulated in all mutations involving proteins NDUFA5 and NDUFB4, both previously identified in ALS, indicating that mitochondrial activity is significantly affected in ALS [45, 46].

Characterization of MSC-EVs

Bone marrow derived MSC-EVs from healthy donor was isolated using differential ultracentrifugation steps at 100,000 x g [47]. Western blot analysis showed that MSC-EVs were positive for the exosomal markers CD9 and CD63 and negative for calnexin, which is an integral protein of endoplasmic reticulum, confirming the purity of EV isolation (**Figure S4**). Nanosight Particle Tracking analysis (NTA) indicates that the nominal EV size is 142 nm and the concentration particle per ml. We have previously shown the size of the EVs by electron microscopy and nanoparticle analysis which ranged between 40 nm and 150 nm, corresponding to exosomal size [47]. In parallel, samples were treated with MSC-EVs for two days and subjected for proteomic analysis. In addition, we injected MSC-EVs lysates for proteomic analysis to characterize the proteome of MSC-EVs. The PCA analysis revealed that the MSC-EV proteome largely differs from the proteome of the neuronal samples, thereby demonstrating that MSC-EVs display an unique proteome compared to the iPSC-derived motor neurons (**Figure S5A**). The MSC-EV-enriched fraction was composed of 1967 proteins with the exosomal markers CD63, CD81 and CD9 being accurately identified. GO analysis of the MSC-EV proteome revealed proteins associated to cellular localization, vesicle-mediated transport and exocytosis (**Figure S5B**).

Proteomic signature after MSC-EV treatment for each ALS mutation

As MSC-EVs are able to promoted neurite growth and branching we aimed to identify the underlying mechanisms associated with this rescue [34]. We followed the proteins that were up or downregulated in ALS for each mutation and highlighted their expression on the volcano plot after EV treatment (ALS+EVs and CTRL+EVs) (**Figure 5A-C, Table S4**). Importantly, levels of the majority of the significantly up- or downregulated proteins in ALS were normalized or changed to opposite direction after treatment with MSC-EVs. In C9ORF72 for example, most of the significantly downregulated proteins (**Figure 3C**) increased their levels upon treatment with MSC-EVs. Likewise, FUS and TDP-43 showed these effects upon MSC-EV treatment. **Figure 5D-F** highlighted the top 10 most up- and downregulated proteins for each mutation and their normalized levels after MSC-EV treatment. Encouragingly, MSC-EVs were able to restore or normalize ALS proteomes,

suggesting a rescue effect by MSC-EVs. In order to determine how MSC-EVs affected the proteome in healthy neurons, control samples were exposed to MSC-EVs (**Table S5**).

Next, common ALS proteome changes upon MSC-EV treatment were analyzed (**Figure 6A-B**). Overall, MSC-EVs treatment upregulated proteins involved in fiber assembly, actin filament assembly and autophagy while downregulated mRNA processes in ALS. As previously shown for mutation-specific protein levels changes upon EVs exposure, overall ALS cells treated with EVs exhibited normalization of their proteome. Importantly, this rescue effect was specific for ALS and not control cells. **Figure 6C** provides an overview of the top 10 most up- and down-regulated proteins and their expression levels after the EV treatment.

Discussion

In this study, we revealed the proteomic signature of the three ALS-susceptibility genes (C9ORF72, FUS and TDP-43) in iPSC-derived motor neurons. We performed mass spectrometry analysis to reveal the underlying molecular mechanisms and demonstrated ALS mutation-specific as well as ALS general proteomic profiles. In addition, we investigated how the proteome changes after MSC-EV treatment. This study revealed a panel of candidate proteins that are selectively affected in ALS. Mutation-specific alterations involving FUS, revealed processes associated with iron ion homeostasis, cellular response to stress, chromosome organization and immune response. Disturbance in cellular homeostasis and stress granules have been characterized before to contribute to ALS-FUS pathogenesis [48, 49]. Associated processes to C9ORF72 only involve proteins targeting ER, cytoplasmic translation, gene expression and mRNA catabolic processes. Increased ER stress was reported previously in ALS-C9ORF72 human brain samples, as well as in iPSC-motor neurons from patients with C9ORF72 mutation [50, 51]. In TDP-43, we demonstrate specific GO terms such as cytoskeleton-dependent transport and mRNA splicing, which was previously described showing its involvement in the pathological context of ALS. Under stress conditions, TDP-43 is able to form cytoplasmic stress granules that impair RNA binding and splicing function which leads to diminished cytoskeleton of the motor neurons [52, 53].
In addition, we demonstrated the top 10 most up- and downregulated proteins across the three mutations. This resulted in several candidate proteins being differentially expressed in the mutations. Interestingly, HSPB1, (upregulated in FUS) is a heat-shock proteins having an important role in various CNS pathologies in clearance of protein aggregates. Multiple studies have shown evidence of upregulation of HSPB1 (termed as HSP25 or HSP27) in symptomatic fALS mice [54-57]. Perhaps most interestingly, iPSC-derived motor neurons in C9ORF72, SOD-1 or TDP-43 showed different expression levels of these heat-shock proteins in response to heat shock indicating that this pathway is induced in ALS in a mutation-specific way [58]. Upregulated RHOB in FUS (slightly upregulated in TDP-43 and C9ORF72) was previously shown to regulate motor neuron death in ALS in a nucleus-to-cytoplasmic transport way [42]. Further research is needed to elicit how this process is affected in the different ALS mutations. In addition, SS18L1 (specifically upregulated in C9ORF72) encodes the calcium-responsive transactivator (CREST), a chromatin regulator gene which is involved in activity-induced dendrite outgrowth. *De novo* mutation in this gene was previously identified in sALS and fALS

patients confirming its contribution to ALS [59]. It was shown that SS18L1-deficient mice display defective dendrite branching, early lethality and motor disturbances suggesting that this protein contributes to the C9ORF72-related pathology [60].

Nonetheless, several aberrant proteome changes were shared between these mutations such as autophagy between FUS and TDP-43. Several studies found autophagy associated proteins being affected with the development of ALS, revealing that protein homeostasis is implicated in the pathogenesis of neurodegenerative disorders, including ALS [61]. It has been established that elevated levels of protein aggregates lead to induction of autophagy. This is a crucial mechanism to clear misfolded and aggregated proteins. Few studies found upregulation of autophagy in degrading spinal motor neurons of ALS patient material and in in the spinal cord of SOD1 mutant mice [62, 63]. In contrast, several studies show decreased levels of autophagy in ALS patient material. C9ORF72 for example is involved in autophagosome formation regulating autophagic flux [64, 65]. Upon C9ORF72 knockdown in murine cortical neurons and human iPSC-derived neurons, autophagy was impaired [64, 66]. Consistent with this finding, conditioned medium from astrocytes differentiated from C9ORF72-derived iPSC lines was applied to HEK293T cells demonstrating decrease in LC3 II levels [67]. ALS-linked mutant FUS show enhanced stress granule accumulation which can be reversed by autophagy activation leading to longer survival in a *Drosophila* model [68]. In line with this, our data show elevated levels of the autophagy-related proteins in FUS (SH3GLB1 and EIG4G2). Furthermore, as TDP-43 was shown to transcriptionally regulate proteins involved in autophagy, we show that in TDP-43, these autophagy-related proteins are downregulated [69].

Since we demonstrated common and ALS-mutation specific pathological mechanisms, we then demonstrated the use of MSC-EVs as elegant therapeutic agents to treat ALS. Previous studies showed that MSC-EVs can improve motor performances in ALS, suggesting the use of MSC-EVs for future clinical use [22, 70]. However, their underlying mechanism of rescue is not established. Here, we highlighted the expression levels of the dysregulated proteins in ALS after treatment with MSC-EVs. We demonstrated that the majority of the dysregulated proteins (mutation specific as well as general ALS proteins) are normalized or changed to opposite direction after treatment with MSC-EVs. Previous study demonstrated that MSC-EVs induce autophagy levels in Parkinson's disease [71]. Our results show altered expression levels of autophagy proteins that normalize after MSC-EV treatment. However, whether MSC-EVs alter autophagy levels in ALS patients have not been described yet.

Although the findings of this study involve only C9ORF72, FUS and TDP-43, further validation is required in larger cohorts to understand the clinical application and robustness of MSC-EVs in ALS. It would be interesting to explore these findings and compare the proteome profile of ALS neurons after treatment with *Riluzole* an *Edaravone* the only approved drug for ALS.

In conclusion, we elucidated a proteomic profile of ALS-susceptibility genes and their expression changes after MSC-EV treatment. Further investigation is required to elucidate these processes in ALS patients after MSC-EV treatment.

Materials and methods

Cell culture

iPSC information and cultivation

The iPSC lines were reprogrammed, characterized, as described elsewhere [39, 72]. FUS (R495QfsX527) and isogenic control lines were kindly provided by Tobias M. Boeckers. C9ORF72 (Hexanucleotide repeat expansion (6-8kb) and isogenic iPSC lines were kindly contributed by Cedars Sinai and TDP-43 (I383T mutation) (provided by Ruxandra Dafinca, Oxford UK [73] and age, sex match control were generated in our lab. The details of the iPSC lines are provided in Table 1.

These obtained ALS-iPSCs and the matched iPSC controls were maintained at 37 °C with 5% CO2 in feeder free conditions. Cells were cultured on Geltrex-coated (Life Technologies, A1413202) dishes, weekly passaged with Trypsin-EDTA (Life technologies) and seeded in Stemflex medium (STEMCELL technologies) with ROCK-inhibitor Y-27632 (4.82 µM, Axon 1683). Medium was replaced every other day. All lines were frequently tested for mycoplasma infection (Lonza, LT07-318). Alll experimental procedures for iPSCs were approved by the medical ethical committee of the University Medical Center Utrecht.

Small molecule directed Spinal Lower motor neuron differentiation

For spinal lower motor neuron differentiation, iPSCs were differentiated according to previously described protocol with some alterations [39]. iPSCs were dissociated with 1mg/ml Dispase (StemCell Technologies) and cultured on Geltrex-coated 6-well plates. The seeding density was optimized per iPSC line depending on its proliferation rate. The following basal medium was prepared and used throughout the differentiation process. Basal medium contained 1:1 mix of DMEM/F12 and Neurobasal supplemented with 1x Sodium Pyruvate, 100uM Non-Essential Amino Acids, 1x GlutaMAX, 1x Penicilin/Streptomycin, 1x N2 supplement, and 1x B27 supplement. Approximately 1-2 days post-seeding, small iPSC colonies received a neuronal differentiation medium containing basal medium supplemented with ascorbic acid (0.4 mM, Santa Cruz), LDN193189 (0.2 µM, Miltenyi Biotec), CHIR99021 (3 mM, Torcris), and SB431542 (10 µM, Stemgent) for 6 days. Medium was replaced every other day. On day 7, base medium consisted of ascorbic acid (0.4 mM), LDN193189 (0.2 µM), CHIR99021 (1 µM), SB431542 (10 µM), Retinoic Acid (RA) (200 nM, Stemgent), Pur (0.5 mM, Stemgent) and cAMP (0.5 µM) was added to the cells for another 6 days. Medium was replaced every day or every other day. On day 12 iPSC were differentiated into the motor neuronal progenitors, which were dissociated with Accutase and put in suspension in basal medium supplemented with ascorbic acid (0.4mM Santa Cruz), cAMP (0.5 µM), retinoic acid (500 nM), and purmorphamine (0.1 µM) for additional 6 days. Medium was replaced every other day. At day 18, cells in suspension were washed in PBS and dissociated with Accutase. After dissociation, motor neurons were plated on PDL/Laminin coated 12-well or 6-well plates at 150.000 and 500.000 cells per well, respectively. Adherent motor neurons were cultured in the base medium supplemented with ascorbic acid (0.4 mM), cAMP (1 µM), BDNF, GDNT and CNTF (10 ng/ml), and BrainXell supplement (diluted

1000 times). Half medium change was performed twice a week. Characterization and treatments were performed at day 24.

Mesenchymal stem cells

Human bone marrow samples were derived from a non-HLA-matched healthy donor and approved by the Dutch Central Committee on Research Involving Human Subjects (CCMO). The bone marrow was separated using a density gradient centrifugation (Lymphoprep, Ais Shield). Bone marrow MSCs were isolated by plastic adherent as described previously [74]. MSCs were cultured in alpha-modified Eagle's medium (α-MEM, Gibco Invitrogen, Carlsbad, CA, USA) supplemented with 1% L-Glutamine (Macopharma), 100 U/mL penicillin (Gibco, Invitrogen), 100 µg/mL streptomycin (Gibco, Invitrogen), 5% human platelet lysate and 10 U/mL heparin [75]. Medium was changed every 3 days and at 80% confluence, cells were washed with PBS, detached with 0.05% trypsin/ethylenediaminetetraacetic acid (EDTA) and passaged to new culture in a 175 cm^2 flask.

Extracellular vesicle isolation

Extracellular vesicles (EVs) were isolated from the MSC culture medium as described previously [76]. First, MSCs were cultured for 48 h in medium which was depleted from EVs by overnight centrifugation at 100,000 x g. Then, we isolated the EVs from the conditioned medium with different centrifugation steps. First, cells were removed by two centrifugations at 200 x g for 10 min. Then, the supernatant was two times centrifuged at 500 x g for 10 min, followed by 10,000 x g for 45 min. Then, vesicles were pelleted by ultracentrifugation at 100,000 x g for 16 h in SW32Ti rotor (Beckman). As last, EVs were washed and pelleted at 100,000 x g overnight in PBS containing 0.5% BSA in SW60 rotor (Beckman). EVs were stored in PBS with 0.5% BSA at -80 °C until use. We treated motor neurons with EVs derived from 4*10^6 MSCs per well for 2 days.

Nanoparticle Tracking Analysis

The size distribution and quantification of isolated EVs was determined using Nanosight NS500 (Marvern, Worcestershire, UK) with the following settings: camera level: 13, slider shutter: 1232, slider gain: 219, detection: 5, autoblur mode for the analysis. Samples were diluted 100, 300, 500, 700, and 1000 times with PBS to reach optimal concentration for instrument linearity.

RNA isolation, cDNA synthesis and qPCR

Cells were lysed using TRIzol (Thermo Fisher, 15596026). Samples were stored at − 80 °C before RNA extraction. RNA was extracted and cDNA prepared as previously described [77]. Primers were designed with PrimerBLAST (NCBI) in such way that they are intron-spanning. The expression fold changes were determined ($2^{-\Delta\Delta CT}$) and normalized with the geomean of the three reference genes *GAPDH*, *BETA-ACTIN* and *TBPQ* (see **Table S6**.). GraphPad Prism, version 8.3.1 was used to prepare graphs (GraphPad Software, San Diego, CA, USA)

Immunocytochemistry

Motor neuronal cultures were fixed at day 24 using 4% paraformaldehyde (PFA; Sigma, P6148) in PBS. Cells were washed with PBS, blocked using 2% BSA, 0.1% Triton X-100 and either 5% goat serum. Antibodies were diluted in a blocking buffer containing 2% BSA, 1% Triton X-100 and 5% goat serum and incubated overnight at 4°C and DNA was labeled using Hoechst (Thermo Fisher, H3570). Images were subsequently captured with confocal microscope. All antibodies, and antibody dilutions are listed in **Table S7**.

Westernblot

Cell pallets were lysed by adding Laemmli sample buffer and incubated for 5 min at 95°C. To determine protein concentration, Bradford-Test was performed according to standard procedures. For SDS-Page and Western blotting, proteins were transferred to polyvinylidene difluoride (PVDF) membrane (Millipore) according to manufactures protocol and blocked in 5% BSA/TBS for 1 h and incubated overnight at 4 °C with the following antibodies: mouse anti-CD9 (1:1000; Biolegend), mouse anti-CD63 (1:1000; Abcam) and rabbit anti-calnexin (1:1000; Abcam). Next day, membranes were washed, incubated with appropriate peroxidase-conjugated secondary antibodies in 5% BSA/TBS for 1 h. After another 3 times washes with TBS, blots were developed by ELC (Amersham Pharmacia).

Sample preparation for mass spectrometry

Samples (n=39) were collected and prepared as indicated before [36]. In short, samples (n=18) not treated with EVs and treated with EVs (n=18) as well as EV samples (n=3) were collected and lysed with lysis buffer containing 1% sodium deoxycholate (SDC), 10 mM tris(2-carboxyethyl)phosphine hydrochloride (TCEP), 40 mM chloroacetamide (CAA), and 100 mM TRIS, pH 8.0 supplemented with phosphatase inhibitor (PhosSTOP, Roche) and protease inhibitor (Complete mini EDTA-free, Roche). Lysate was sonicated using a Bioruptor (Diagenode) and centrifuges at 2500 g for 10 min at 4 °C. All samples were assessed for protein concentration using the bicinchoninic acid (BCA) assay kit (Waltham MA, USA) according to manufacturer's protocol. Reduction and alkylation was done with 4 mM DTT (25 min at 56 °C) followed with 8 mM iodoacetamide (30 min at room temperature in the dark). Proteins were then digested into peptides by LysC (protein-enzyme ratio 1:50) at 37 °C for 4 h and trypsin (protein-enzyme ratio 1:50) at 37 °C for 16 h. Peptides were then desalted using C18 solid phase extraction cartridges (Waters), dried in vacuum and resuspended in 50 mM triethylammonium bicarbonate at a final concentration of 5 mg/mL.

Mass spectrometry analysis

Mass spectrometry was performed on Orbitrap Fusion Lumos (Thermo Fisher Scientific) coupled to an Agilent 1290 HPLC system (Agilent Technologies). We used a double-frit trap column of 20 mm × 100 µm inner diameter (ReproSil C18, Dr Maisch GmbH, Ammerbuch, Germany) to separate peptides. Then we used a 40 cm × 50 µm inner diameter analytical column (ReproSil Pur C18-AQ, Dr Maisch GmbH, Ammerbuch, Germany) for further separation. Trapping was performed at 5 µl/min in 0.1 M acetic acid

in H_2O for 10 min, and the analytical separation was done at 300 nl/min for 2 h by increasing the concentration of 0.1 M acetic acid in 80% acetonitrile (*v*/*v*). We operated the mass spectrometer in a data-dependent mode, automatically switching between MS and MS/MS. Full-scan MS spectra were acquired in the Orbitrap from m/z 350–1500 with a resolution of 60,000 FHMW, automatic gain control (AGC) target of 200,000 and maximum injection time of 50 ms. Then, ten most intense precursors at a threshold above 5000 were selected with an isolation window of 1.2 Da after accumulation to a target value of 30,000 (maximum injection time was 115 ms). Higher-energy collisional dissociation (HCD) was carried out for fragmentation with collision energy of 38% and activation time of 0.1 ms. Fragment ion analysis was performed on Orbitrap with resolution of 60,000 FHMW and a low mass cut-off setting of 120 m/z.

Data processing

MS raw files were processed using Proteome Discoverer software (version 2.2, Thermo Scientific). Peak list was searched using the Swissprot database (version 2014_08) with the search engine Sequest HT. The following parameters were used. Trypsin was specified as enzyme, and up to two missed cleavages were allowed. Taxonomy was set for Homo sapiens, and precursor mass tolerance precursor mass tolerance was set to 10 ppm with 0.6 Da fragment mass tolerance. Carbamidomethylation on cysteine residues (+57.021 Da) was set to fixed modification. Dynamic modifications were set for Oxidation of methionine residues (+15.995 Da), N termini acetylation (+42.011 Da) and Met-loss (-131.040 Da) and Met-loss (-89.030 Da). The results were filtered with a percolator to adjust the peptide-spectrum matches to a FDR below 1%.

Data visualization

Normalized protein and peptide abundances were extracted from PD2.2 and further analyzed using the open software PERSEUS environment for statistical and bioinformatics analysis and to generate the plots and figures. For several plots, we also used GraphPad Prism (version 7.04). Functional analysis to enrich to GO terms was done on Enrichr (Maayanlab.com)

Statistical analysis

Volcano plots were generated for the indicated conditions with a cut-off for proteins being up- or downregulated with a p value ≤ 0.1 and ≥ 1.5-fold change difference. To study protein subsets consistently dysregulated in all ALS mutations (here, C9ORF72, FUS and TDP-43), we grouped all ALS samples and all CTRL samples together. A volcano plot was generated, and proteins were considered significantly up- or downregulated with a p value ≤ 0.1 and ≥ 1.5-fold change difference.

Data availability

All mass spectrometry proteomics data have been deposited to the ProteomeXchange Consortium via the PRIDE partner repository with the data set identifier PXD034824.

Username: reviewer_pxd034824@ebi.ac.uk
Password: IDoEOWRj

Figure 1.

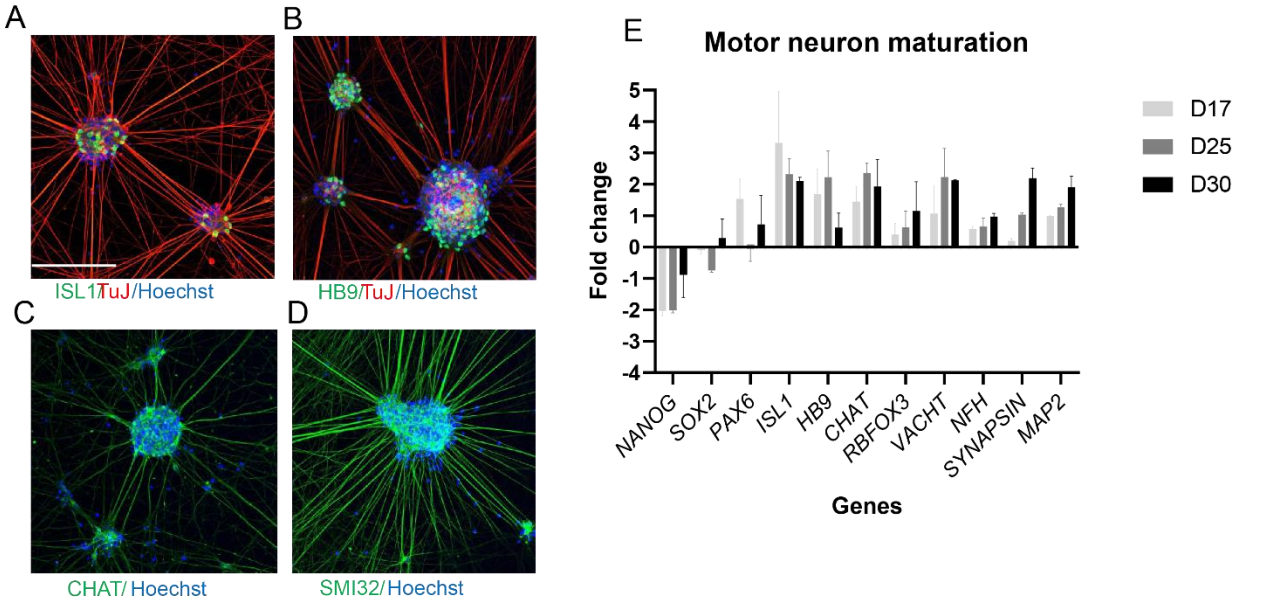

Figure 2

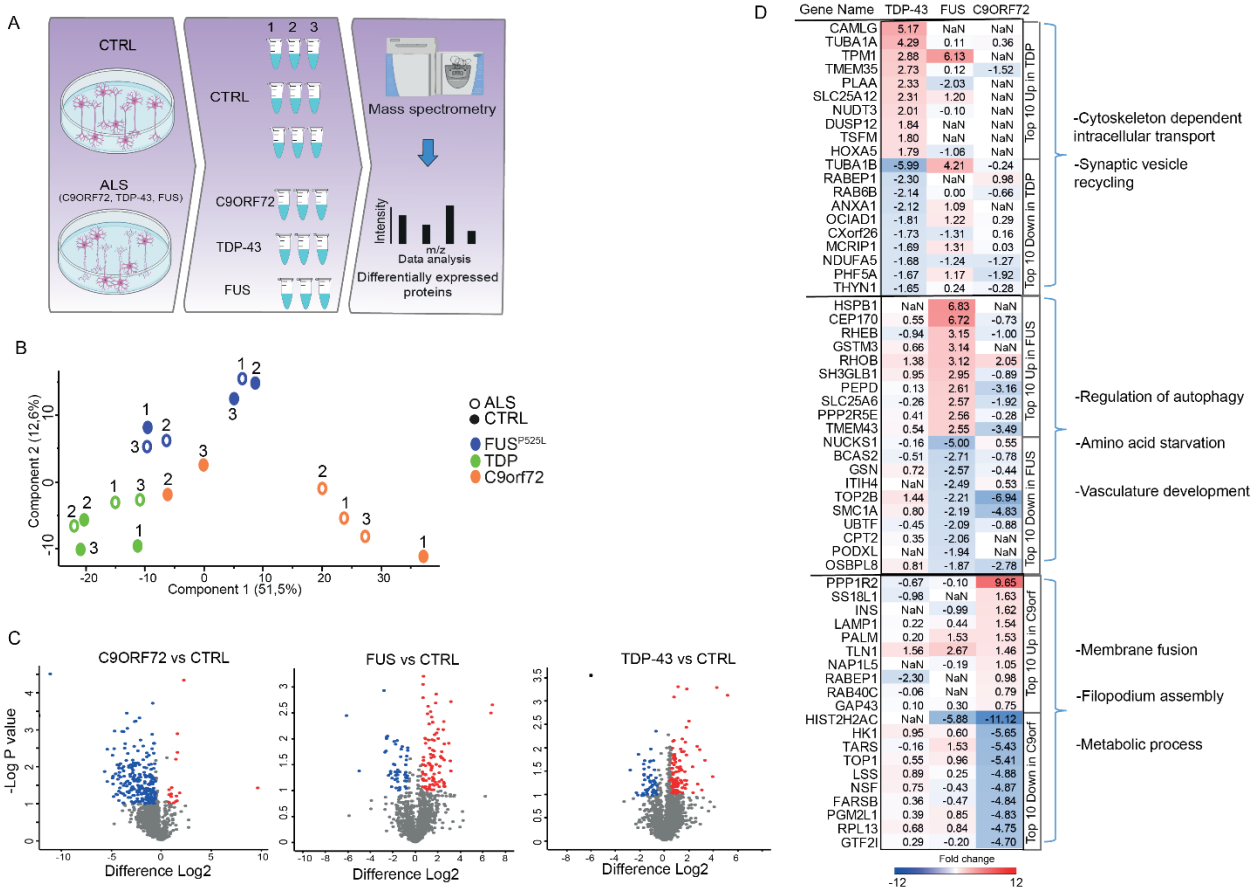

Figure 3

A

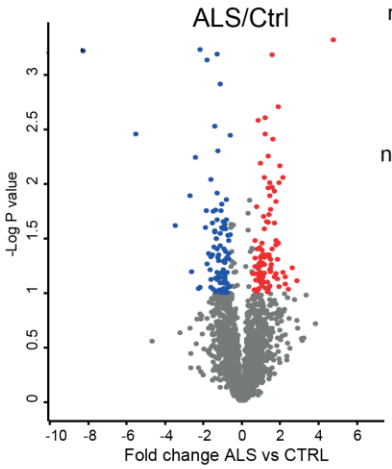

B

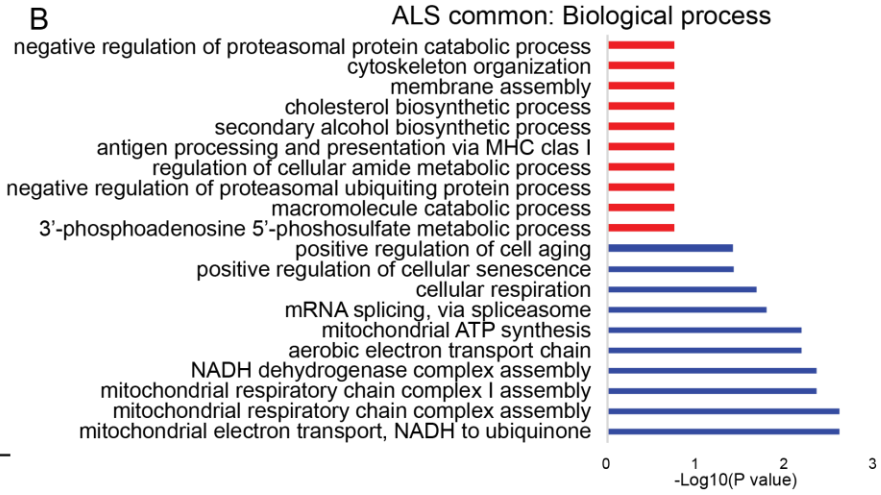

C

Gene name	ALS/Ctrl
MYO6	2.61
FLNC	2.26
RHOB	1.96
GNAQ	1.70
POLR2B	1.69
TECR	1.56
GMPPB	1.53
EIF4G2	1.49
SEC23A	1.48
SCAMP1	1.43
NDUFAB1	-1.52
ACBD7	-1.59
PSMB3	-1.61
ACTR3	-1.61
IRF2BPL	-1.63
ACBD6	-1.67
EEF1D	-1.81
PPM1A	-1.83
HTATSF1	-1.88
HIST2H2AC	-8.28

Cellular response to radiation
Canonical Wnt signaling
Macromolecule biosynthetic process
Actin filament organization

Figure 4

A

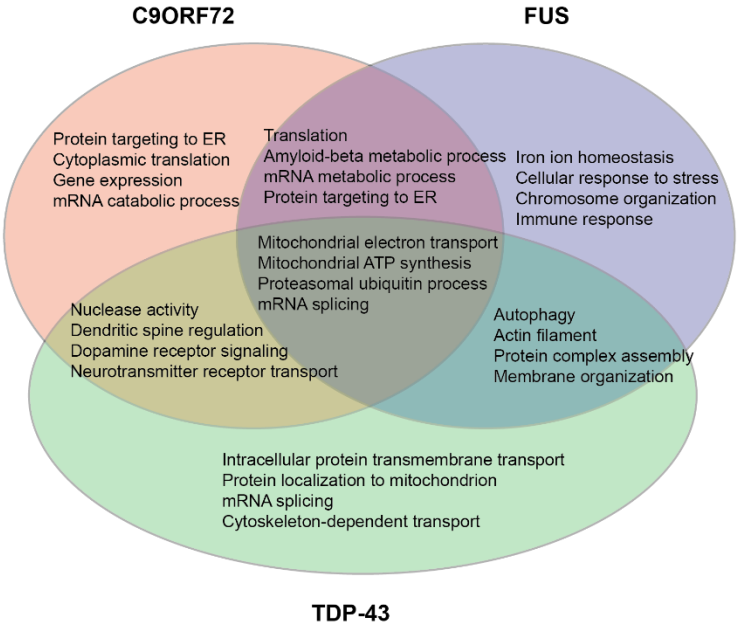

B

Proteins targeting to ER

Protein	C9ORF72
RPL3	-3,251
RPS8	-3,806
RPL23	-2,823
RPL22	-1,268
RPL13A	-2,645
SRP14	-1,050
RPL9	-3,227
RPL7	-3,196
RPS19	-0,609
RPS18	-1,296
RPS3	-2,554
RPL35	-2,381
RPL13	-4,753
RPS20	-0,770
RPL28	-2,131

Intracellular protein transmembrane transport

Protein	TDP-43
CHCHD4	-0,818
DNAJC19	1,144
TIMM44	0,946
SEC61B	0,818

Cellular response to stress

Protein	FUS
PTGES3	1,147
CHORFC1	-1,832
RAE1	-0,766
MANF	0,952
EIF4G1	1,519

Translation

Protein	FUS	C9ORF72
RPS27	-1,250	-2,057
RPL34	1,453	-3,796
APEH	1,829	-1,643

Autophagy

Protein	TDP-43	FUS
SH3GLB1	0,951	2,951
EIF4G2	0,660	2,530

Neurotransmitter transport and nuclease activity

Protein	TDP-43	C9ORF72
TERF2IP	-0,894	-1,023
HMGB2	-0,782	-1,130
RABEP1	-2,296	0,981
SS18L1	-0,983	1,629
H2AFY	0,720	-3,820
VPS35	0,876	-4,236
CYB5R3	0,721	-2,640
GART	0,601	-3,473
RAB21	1,050	-2,627
ATAT1	0,793	-1,174

Mitochondrial electron transport

Protein	TDP-43	FUS	C9ORF72
NDUFA5	-1,677	-1,235	-1,267
NDUFB4	0,970	3,728	1,367

Figure 5

A

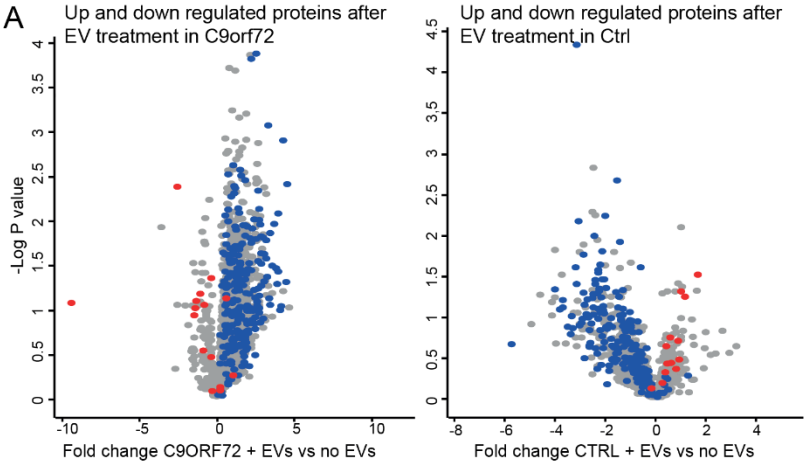

D

Gene Name	C9ORF72	+EVs	
PPP1R2	9.65	-9.36	Top 10 Up inC9ORF72
SS18L1	1.63	-0.83	
INS	1.62	NaN	
LAMP1	1.54	-0.31	
PALM	1.53	0.2	
TLN1	1.46	-1.1	
NAP1L5	1.05	0.61	
RABEP1	0.98	1.07	
RAB40C	0.79	-1.36	
GAP43	0.75	-0.33	
HIST2H2AC	-11.12	11.74	Top 10 Down in C9ORF72
HK1	-5.65	3.96	
TARS	-5.43	4.45	
TOP1	-5.41	3.81	
LSS	-4.88	3.46	
NSF	-4.87	4.09	
FARSB	-4.84	3.26	
PGM2L1	-4.83	3.95	
RPL13	-4.75	2.06	
GTF2I	-4.70	2.97	

Fold change
-12 12

B

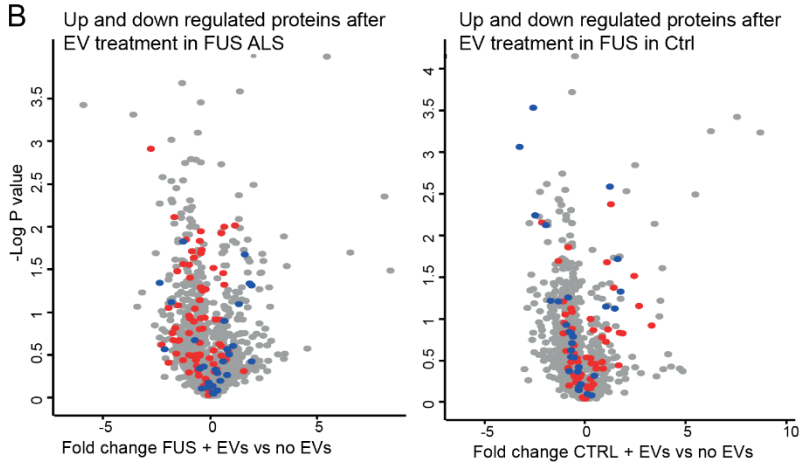

E

Gene Name	FUS	+EVs	
HSPB1	6.83	0.58	Top 10 Up inFUS
CEP170	6.72	-6.05	
RHEB	3.15	-2.77	
GSTM3	3.14	-0.99	
RHOB	3.12	-0.99	
SH3GLB1	2.95	-0.68	
PEPD	2.61	0.02	
SLC25A6	2.57	-0.33	
PPP2R5E	2.56	-2.27	
TMEM43	2.55	-1.94	
NUCKS1	-5.00	-0.07	Top 10 Down in FUS
BCAS2	-2.71	NaN	
GSN	-2.57	NaN	
ITIH4	-2.49	1.82	
TOP2B	-2.21	-0.76	
SMC1A	-2.19	-0.09	
UBTF	-2.09	1.04	
CPT2	-2.06	NaN	
PODXL	-1.94	NaN	
OSBPL8	-1.87	1.91	

Fold change
-7 7

C

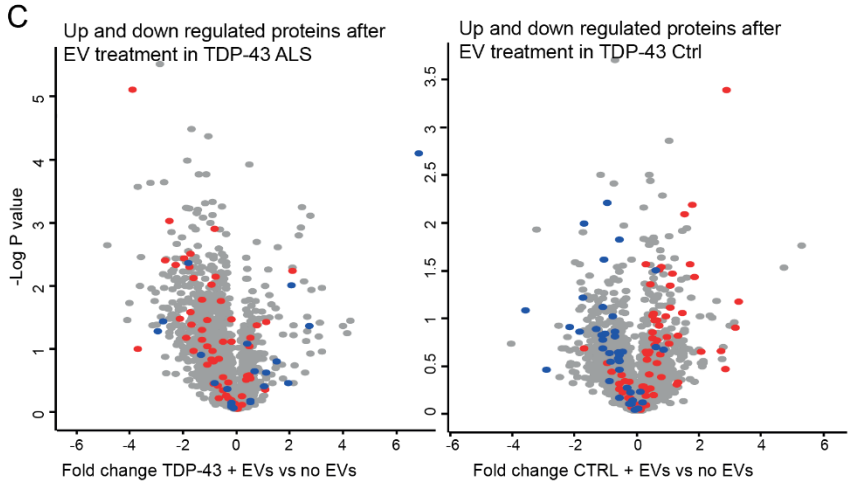

F

Gene Name	TDP-43	+EVs	
CAMLG	5.17	NaN	Top 10 Up in TDP-43
TUBA1A	4.29	-3.9	
TPM1	2.88	-2.47	
TMEM35	2.73	0.11	
PLAA	2.33	-3.69	
SLC25A12	2.31	NaN	
NUDT3	2.01	NaN	
DUSP12	1.84	NaN	
TSFM	1.80	NaN	
HOXA5	1.79	0.2	
TUBA1B	-5.99	6.83	Top 10 Down in TDP-43
RABEP1	-2.30	-2.96	
RAB6B	-2.14	-0.18	
ANXA1	-2.12	0.96	
OCIAD1	-1.81	1.03	
CXorf26	-1.73	1.95	
MCRIP1	-1.69	0.53	
NDUFA5	-1.68	0.96	
PHF5A	-1.67	NaN	
THYN1	-1.65	-0.17	

Fold change
-7 7

Figure 6

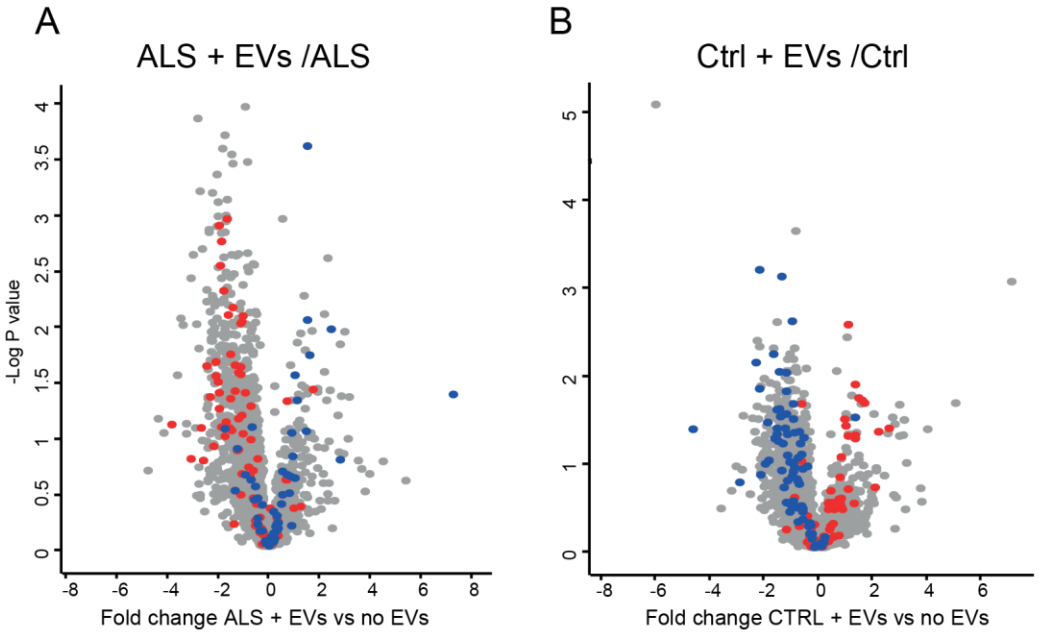

C

Gene name	ALS/Ctrl	+EVs
MYO6	2.61	-3.83
FLNC	2.26	-2.42
RHOB	1.96	-1.53
GNAQ	1.70	-1.93
POLR2B	1.69	-2.29
TECR	1.56	-2.07
GMPPB	1.53	-1.06
EIF4G2	1.49	-2.00
SEC23A	1.48	-1.74
SCAMP1	1.43	-1.95
NDUFAB1	-1.52	1.07
ACBD7	-1.59	-0.54
PSMB3	-1.61	0.26
ACTR3	-1.61	-0.11
IRF2BPL	-1.63	1.07
ACBD6	-1.67	2.82
EEF1D	-1.81	0.37
PPM1A	-1.83	0.32
HTATSF1	-1.88	-1.08
HIST2H2AC	-8.28	7.28

Cellular response to radiation
Canonical Wnt signaling
Macromolecule biosynthetic process
Actin filament organization

Figure S1

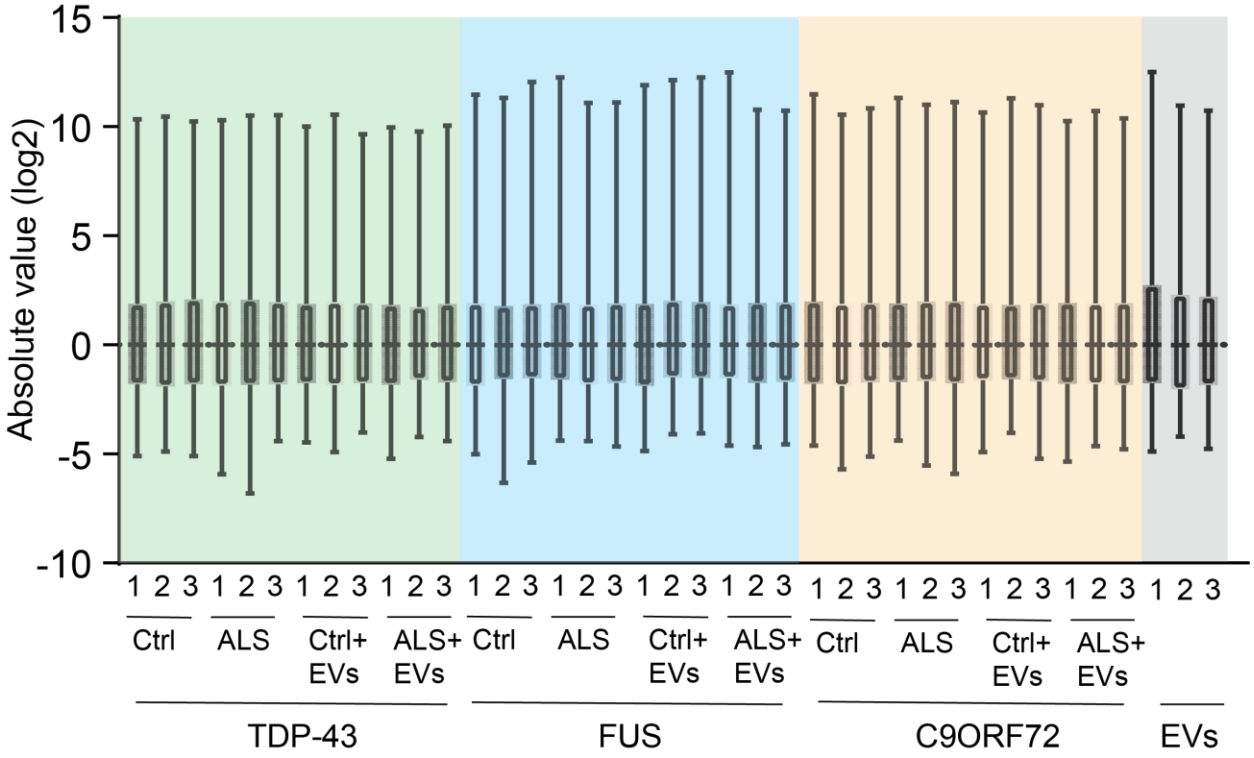
Absolute value (log2)
15
10
5
0
-5
-10
1 2 3
Ctrl
ALS
Ctrl+ EVs
ALS+ EVs
TDP-43
FUS
C9ORF72
EVs

Figure S2

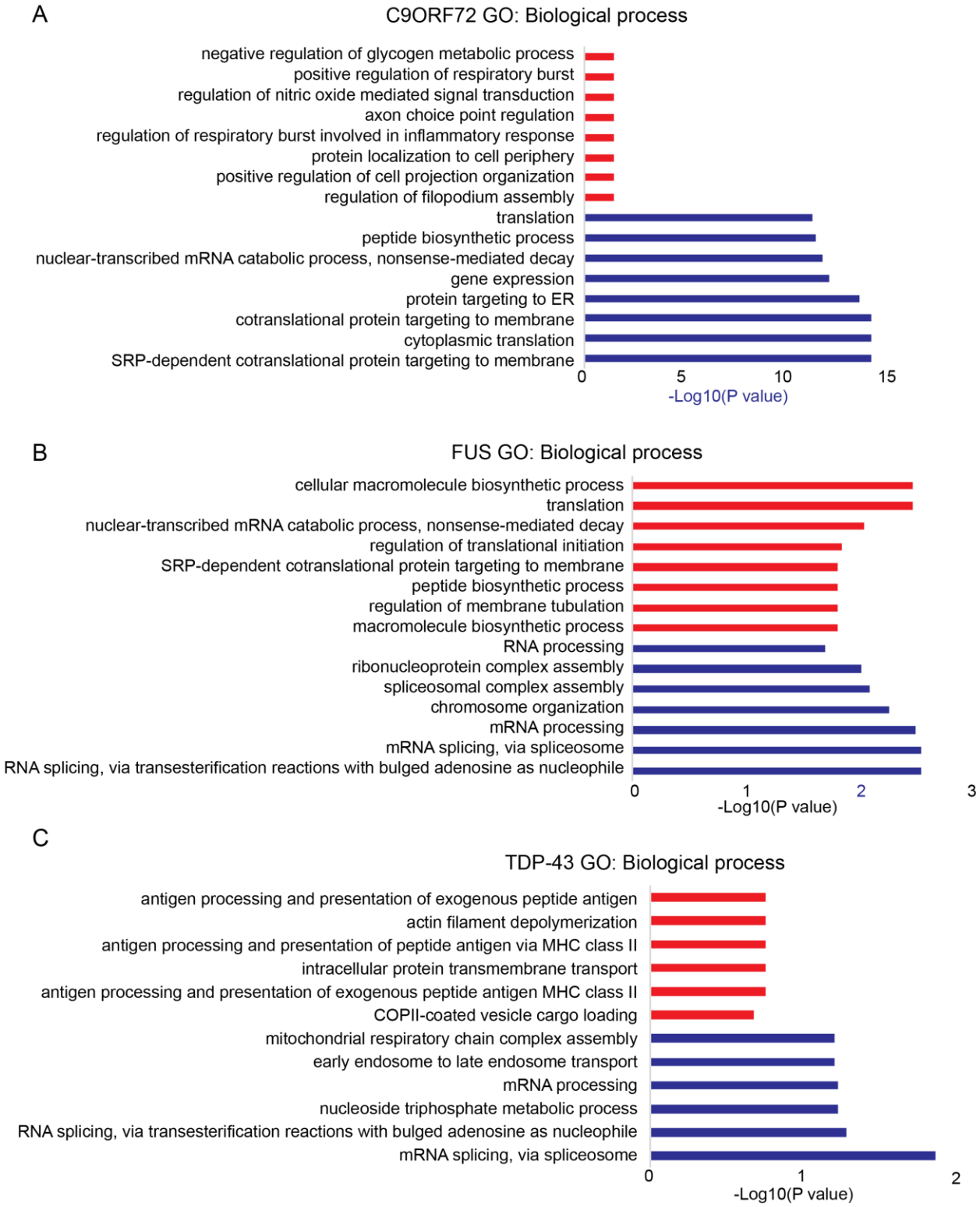
A
C9ORF72 GO: Biological process
negative regulation of glycogen metabolic process
positive regulation of respiratory burst
regulation of nitric oxide mediated signal transduction
axon choice point regulation
regulation of respiratory burst involved in inflammatory response
protein localization to cell periphery
positive regulation of cell projection organization
regulation of filopodium assembly
translation
peptide biosynthetic process
nuclear-transcribed mRNA catabolic process, nonsense-mediated decay
gene expression
protein targeting to ER
cotranslational protein targeting to membrane
cytoplasmic translation
SRP-dependent cotranslational protein targeting to membrane
0
5
10
15
-Log10(P value)
B
FUS GO: Biological process
cellular macromolecule biosynthetic process
translation
nuclear-transcribed mRNA catabolic process, nonsense-mediated decay
regulation of translational initiation
SRP-dependent cotranslational protein targeting to membrane
peptide biosynthetic process
regulation of membrane tubulation
macromolecule biosynthetic process
RNA processing
ribonucleoprotein complex assembly
spliceosomal complex assembly
chromosome organization
mRNA processing
mRNA splicing, via spliceosome
RNA splicing, via transesterification reactions with bulged adenosine as nucleophile
0
1
2
3
-Log10(P value)
C
TDP-43 GO: Biological process
antigen processing and presentation of exogenous peptide antigen
actin filament depolymerization
antigen processing and presentation of peptide antigen via MHC class II
intracellular protein transmembrane transport
antigen processing and presentation of exogenous peptide antigen MHC class II
COPII-coated vesicle cargo loading
mitochondrial respiratory chain complex assembly
early endosome to late endosome transport
mRNA processing
nucleoside triphosphate metabolic process
RNA splicing, via transesterification reactions with bulged adenosine as nucleophile
mRNA splicing, via spliceosome
0
1
2
-Log10(P value)

Figure S3

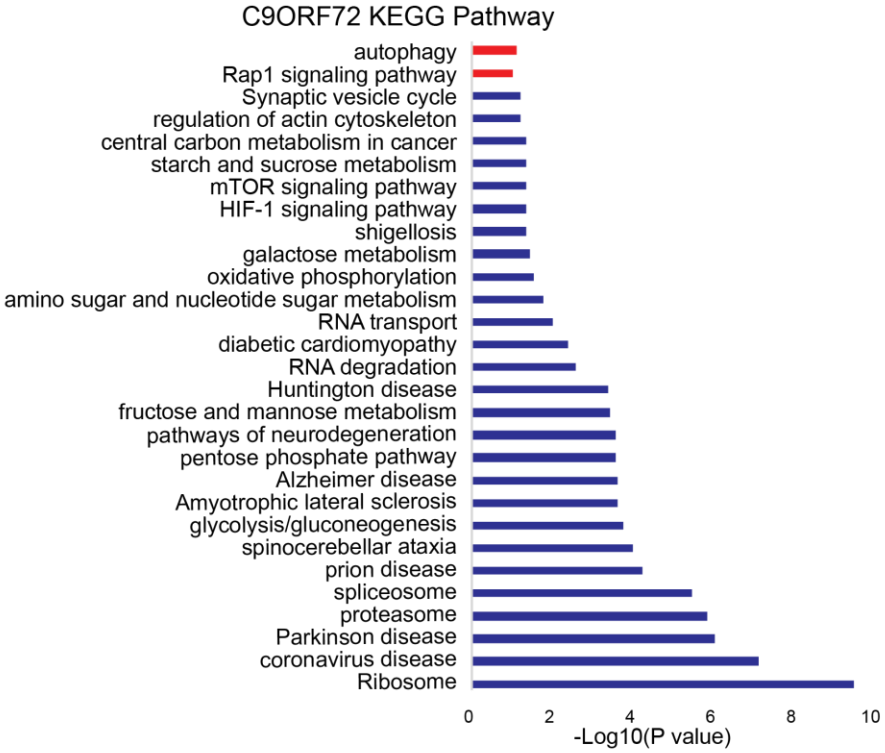

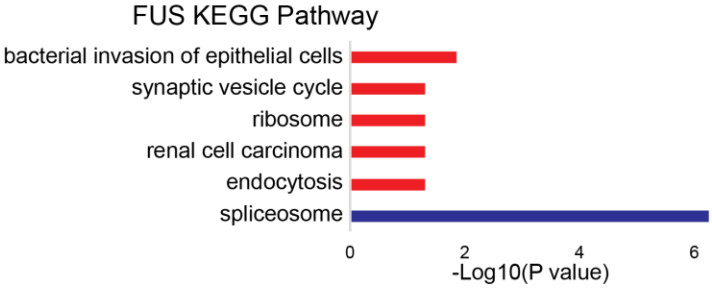

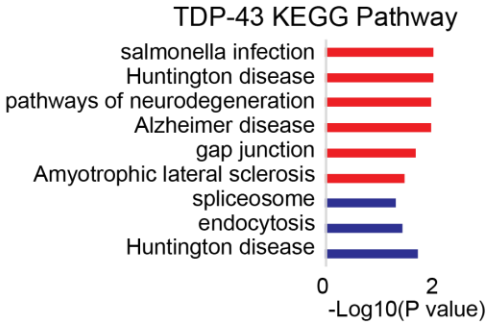

Figure S4

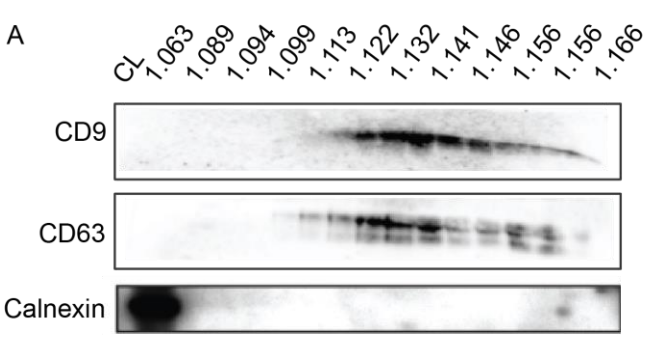

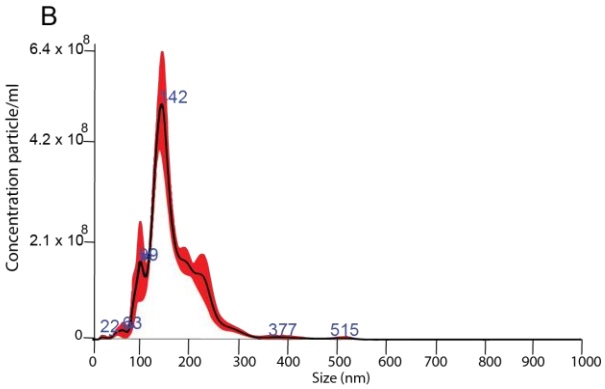

Figure S5

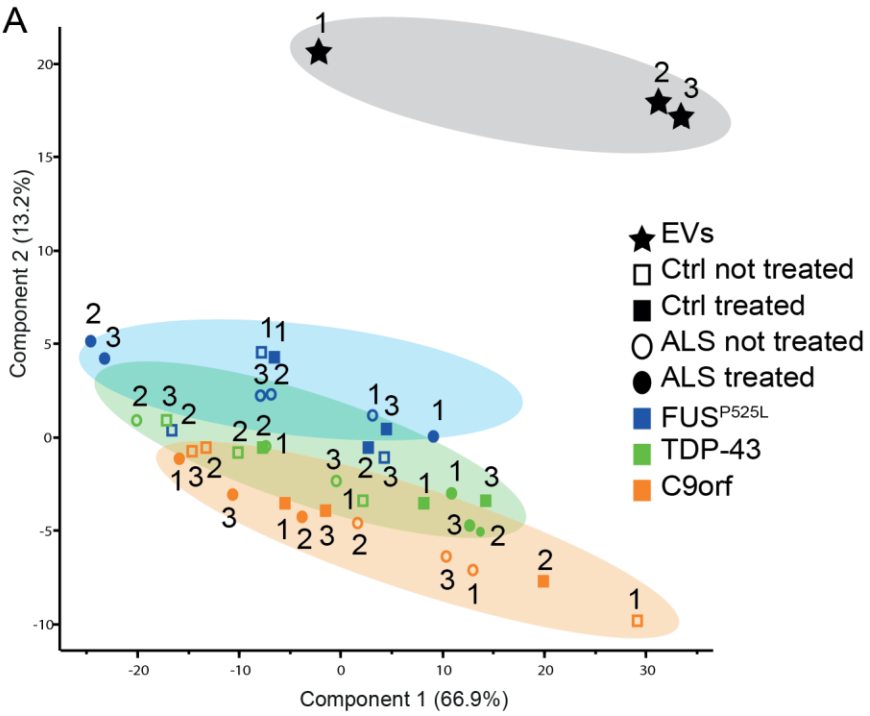
A
Component 2 (13.2%)
Component 1 (66.9%)
EVs
Ctrl not treated
Ctrl treated
ALS not treated
ALS treated
FUSP525L
TDP-43
C9orf

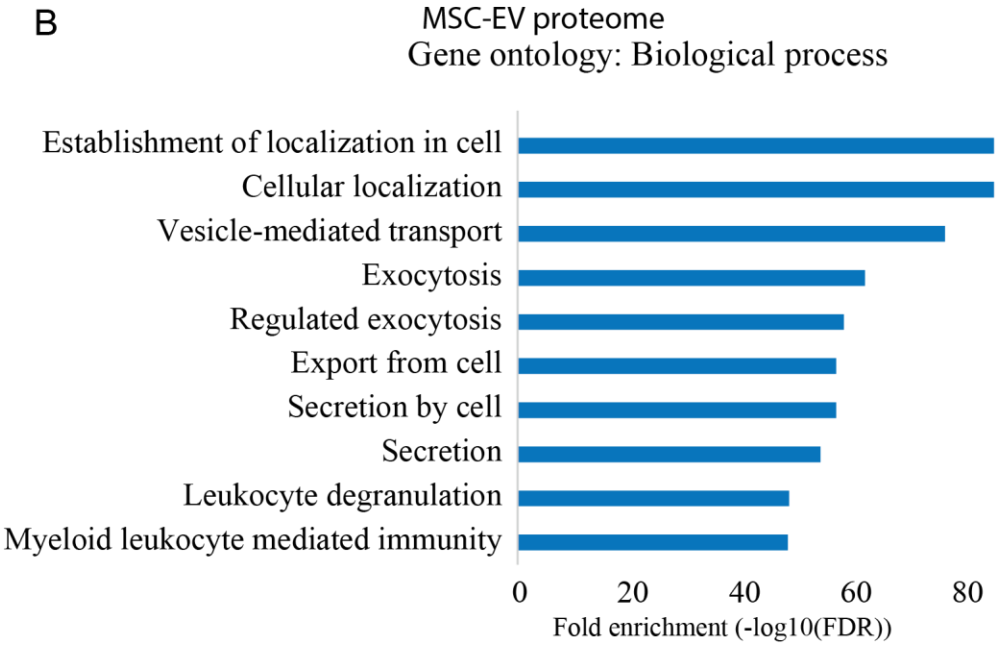
B
MSC-EV proteome
Gene ontology: Biological process
Establishment of localization in cell
Cellular localization
Vesicle-mediated transport
Exocytosis
Regulated exocytosis
Export from cell
Secretion by cell
Secretion
Leukocyte degranulation
Myeloid leukocyte mediated immunity
0
20
40
60
80
Fold enrichment (-log10(FDR))

Figure legends

Figure 1: Characterization of iPSC-derived motor neurons. Motor neurons were differentiated for 25 days and immunostained for motor neuron markers (**A**) ISL1 (in green) and TuJ (in red), (**B**) HB9 (in green) and TuJ (in red), (**C**) CHAT (in green), (**D**) SMI32 (in green), and Hoechst (in blue), the scale bar is 250 µm. (**E**) mRNA expression levels of induced pluripotent stem cells (iPSC), motor neuron differentiated for 17, 25, and 30 days. Expression of markers of neural stem cells (NANOG, SOX2, PAX6), motor neurons (ISL1, HB9, CHAT, RBFOX3, VACHT, NFH), and mature motor neurons (SYNAPSIN, MAP2). Graphs shows fold change values as compared to expression in iPSCs.

Figure 2: Proteomic analysis. (**A**) Experimental workflow of iPSC-derived motor neurons carrying C9ORF72, FUS or TDP-43 and their CTRL motor neurons. Samples were processed with MS-based proteomics for the proteomic signature. (**B**) PCA analysis of the proteome of the samples analyzed. (**C**) Volcano plot demonstrating proteins differentially expressed in TDP-43, FUS and C9ORF72 compared to their CTRLs. The x-as represents the log2-fold change and the y-as the -log10 (p-value). Threshold for significant proteins is chosen for p-value cut-off (0.1) and fold change ≥ 1.5. Blue color indicates for downregulated proteins and red for upregulated proteins. (**D**) Heatmap highlighting the top 10 most up- and downregulated proteins for each mutation.

Figure 3: Common ALS processes. (**A**) Volcano plot demonstrating proteins differentially regulated in ALS (C9ORF72, FUS and TDP-43) compared to CTRL. The x-as represents the log2-fold change and the y-as the -log10 (p-value). Threshold for significant proteins is chosen for p-value cut-off (0.1) and fold change ≥ 1.5. Blue color indicates for downregulated proteins and red for upregulated proteins. (**B**) Gene ontology analysis with respect to biological process of the significant proteins. (**C**) Top ten most up- and downregulated proteins in ALS and their biological processes.

Figure 4: Summary of highly dysregulated processes. (**A**) Venn diagram summarizing the most dysregulated proteins for each mutation (C9ORF72, FUS and TDP-43) as well as shared between each other. (**B**) Biological processes highly dysregulated in ALS. Protein expression levels are log2 fold change values.

Figure 5: Follow up mutation specific altered proteins after EV treatment. (**A**). Volcano plot demonstrating proteins differentially regulated in C9ORF72 treated with EVs compared to non-treated cells. Proteins significantly regulated in C9ORF72 compared to CTRL are shown in red (which were upregulated) and in blue (which were downregulated).(**B**) in FUS treated with EVs compared to non-treated cells. (**C**) in TDP-43 treated with EVs compared to non-treated cells. (**D**) Top ten most up- and downregulated proteins in C9ORF72 (**E**) in FUS (**F**) in TDP-43 and their expression levels after EV treatment.

Figure 6: Follow up general ALS altered proteins after EV treatment (**A**) Volcano plot demonstrating proteins differentially regulated in ALS (C9ORF72, FUS and TDP-

43) treated with EVs compared to non-treated cells. (**B**) Proteins that were significantly dysregulated in ALS compared to CTRL are shown in red (which were upregulated) and in blue (which were downregulated) (**C**). Top ten most up- and downregulated proteins in ALS and their expression levels after EV treatment.

Figure S1: Box plot. Log 2 transformed data of each sample.

Figure S2: Gene ontology analysis. (**A**). Gene ontology analysis with respect to biological process of the significant proteins derived from volcano plot from C9ORF72. (**B**) from FUS. (**C**) from TDP-43. Red indicates the upregulated and blue the downregulated biological processes.

Figure S3: KEGG pathway analysis. (**A**). KEGG pathway analysis of the significant proteins derived from volcano plot from C9ORF72. (**B**) from FUS. (**C**) from TDP-43. Red indicates the upregulated and blue the downregulated pathways.

Figure S4: Characterization of MSC-EVs. (**A**) MSC-EVs are positive for the exosomal markers CD63, CD9 and are negative for the exosome-negative marker Calnexin. (**B**) Nanosight Particle Tracking Analysis derived from 5 measurements showing that the nominal size of these vesicles is 142 nm. Color red indicates error bars of the mean.

Figure S5: MSC-EVs proteomic analysis. (**A**) PCA analysis of the proteome of all samples analyzed. (**B**) Gene ontology analysis with respect to biological processes of MSC-EV proteome.

Reference

1. Brown, R.H. and A. Al-Chalabi, *Amyotrophic Lateral Sclerosis.* N Engl J Med, 2017. **377**(2): p. 162-172.
2. van Es, M.A., et al., *Amyotrophic lateral sclerosis.* Lancet, 2017. **390**(10107): p. 2084-2098.
3. Chiò, A., et al., *Global Epidemiology of Amyotrophic Lateral Sclerosis: A Systematic Review of the Published Literature.* Neuroepidemiology, 2013. **41**(2): p. 118-130.
4. Xu, L., et al., *Global variation in prevalence and incidence of amyotrophic lateral sclerosis: a systematic review and meta-analysis.* Journal of Neurology, 2020. **267**(4): p. 944-953.
5. Andersen, P.M. and A. Al-Chalabi, *Clinical genetics of amyotrophic lateral sclerosis: what do we really know?* Nat Rev Neurol, 2011. **7**(11): p. 603-15.
6. Al-Chalabi, A., L.H. van den Berg, and J. Veldink, *Gene discovery in amyotrophic lateral sclerosis: implications for clinical management.* Nat Rev Neurol, 2017. **13**(2): p. 96-104.
7. DeJesus-Hernandez, M., et al., *Expanded GGGGCC hexanucleotide repeat in noncoding region of C9ORF72 causes chromosome 9p-linked FTD and ALS.* Neuron, 2011. **72**(2): p. 245-56.
8. Renton, A.E., et al., *A hexanucleotide repeat expansion in C9ORF72 is the cause of chromosome 9p21-linked ALS-FTD.* Neuron, 2011. **72**(2): p. 257-68.
9. Rosen, D.R., et al., *Mutations in Cu/Zn superoxide dismutase gene are associated with familial amyotrophic lateral sclerosis.* Nature, 1993. **362**(6415): p. 59-62.
10. Kwiatkowski, T.J., Jr., et al., *Mutations in the FUS/TLS gene on chromosome 16 cause familial amyotrophic lateral sclerosis.* Science, 2009. **323**(5918): p. 1205-8.
11. Neumann, M., et al., *Ubiquitinated TDP-43 in frontotemporal lobar degeneration and amyotrophic lateral sclerosis.* Science, 2006. **314**(5796): p. 130-3.
12. Burk, K. and R.J. Pasterkamp, *Disrupted neuronal trafficking in amyotrophic lateral sclerosis.* Acta Neuropathol, 2019. **137**(6): p. 859-877.
13. Swinnen, B., W. Robberecht, and L. Van Den Bosch, *RNA toxicity in non-coding repeat expansion disorders.* Embo j, 2020. **39**(1): p. e101112.
14. Wong, W., *The role of managed care professionals in improving care for patients with ALS.* Am J Manag Care, 2020. **26**(9 Suppl): p. S198-s205.
15. Meamar, R., et al., *Stem cell therapy in amyotrophic lateral sclerosis.* Journal of Clinical Neuroscience, 2013. **20**(12): p. 1659-1663.
16. Marconi, S., et al., *Systemic treatment with adipose-derived mesenchymal stem cells ameliorates clinical and pathological features in the amyotrophic lateral sclerosis murine model.* Neuroscience, 2013. **248**: p. 333-343.
17. Marconi, S., et al., *Human adipose-derived mesenchymal stem cells systemically injected promote peripheral nerve regeneration in the mouse model of sciatic crush.* Tissue Engineering Part A, 2012. **18**(11-12): p. 1264-1272.
18. Bonafede, R. and R. Mariotti, *ALS pathogenesis and therapeutic approaches: the role of mesenchymal stem cells and extracellular vesicles.* Frontiers in cellular neuroscience, 2017. **11**: p. 80.
19. Spejo, A.B., et al., *Neuroprotection and immunomodulation following intraspinal axotomy of motoneurons by treatment with adult mesenchymal stem cells.* J Neuroinflammation, 2018. **15**(1): p. 230.
20. Boucherie, C., et al., *Chimerization of astroglial population in the lumbar spinal cord after mesenchymal stem cell transplantation prolongs survival in a rat model of amyotrophic lateral sclerosis.* J Neurosci Res, 2009. **87**(9): p. 2034-46.
21. Bonafede, R. and R. Mariotti, *ALS Pathogenesis and Therapeutic Approaches: The Role of Mesenchymal Stem Cells and Extracellular Vesicles.* Frontiers in Cellular Neuroscience, 2017. **11**.

22. Bonafede, R., et al., *Exosome derived from murine adipose-derived stromal cells: Neuroprotective effect on in vitro model of amyotrophic lateral sclerosis.* Exp Cell Res, 2016. **340**(1): p. 150-8.
23. Bruno, S., et al., *Microvesicles derived from mesenchymal stem cells enhance survival in a lethal model of acute kidney injury.* PLoS One, 2012. **7**(3): p. e33115.
24. Lai, R.C., et al., *Exosome secreted by MSC reduces myocardial ischemia/reperfusion injury.* Stem Cell Res, 2010. **4**(3): p. 214-22.
25. Zhang, B., et al., *Mesenchymal stem cells secrete immunologically active exosomes.* Stem Cells Dev, 2014. **23**(11): p. 1233-44.
26. Raposo, G. and W. Stoorvogel, *Extracellular vesicles: exosomes, microvesicles, and friends.* J Cell Biol, 2013. **200**(4): p. 373-83.
27. van Niel, G., G. D'Angelo, and G. Raposo, *Shedding light on the cell biology of extracellular vesicles.* Nat Rev Mol Cell Biol, 2018. **19**(4): p. 213-228.
28. Zaborowski, M.P., et al., *Extracellular Vesicles: Composition, Biological Relevance, and Methods of Study.* Bioscience, 2015. **65**(8): p. 783-797.
29. Lötvall, J., et al., *Minimal experimental requirements for definition of extracellular vesicles and their functions: a position statement from the International Society for Extracellular Vesicles.* J Extracell Vesicles, 2014. **3**: p. 26913.
30. Valadi, H., et al., *Exosome-mediated transfer of mRNAs and microRNAs is a novel mechanism of genetic exchange between cells.* Nat Cell Biol, 2007. **9**(6): p. 654-9.
31. Williams, C., et al., *Glycosylation of extracellular vesicles: current knowledge, tools and clinical perspectives.* J Extracell Vesicles, 2018. **7**(1): p. 1442985.
32. Collino, F., et al., *Microvesicles derived from adult human bone marrow and tissue specific mesenchymal stem cells shuttle selected pattern of miRNAs.* PLoS One, 2010. **5**(7): p. e11803.
33. Varderidou-Minasian, S. and M.J. Lorenowicz, *Mesenchymal stromal/stem cell-derived extracellular vesicles in tissue repair: challenges and opportunities.* Theranostics, 2020. **10**(13): p. 5979-5997.
34. Lopez-Verrilli, M.A., et al., *Mesenchymal stem cell-derived exosomes from different sources selectively promote neuritic outgrowth.* Neuroscience, 2016. **320**: p. 129-39.
35. Xin, H., et al., *Exosome-mediated transfer of miR-133b from multipotent mesenchymal stromal cells to neural cells contributes to neurite outgrowth.* Stem Cells, 2012. **30**(7): p. 1556-64.
36. Varderidou-Minasian, S., et al., *Spinal Muscular Atrophy Patient iPSC-Derived Motor Neurons Display Altered Proteomes at Early Stages of Differentiation.* ACS Omega, 2021. **6**(51): p. 35375-35388.
37. Varderidou-Minasian, S., et al., *Quantitative proteomic analysis of Rett iPSC-derived neuronal progenitors.* Molecular Autism, 2020. **11**(1): p. 38.
38. Higelin, J., et al., *FUS Mislocalization and Vulnerability to DNA Damage in ALS Patients Derived hiPSCs and Aging Motoneurons.* Frontiers in cellular neuroscience, 2016. **10**: p. 290-290.
39. Du, Z.-W., et al., *Generation and expansion of highly pure motor neuron progenitors from human pluripotent stem cells.* Nature communications, 2015. **6**: p. 6626-6626.
40. Saris, C.G.J., et al., *Weighted gene co-expression network analysis of the peripheral blood from Amyotrophic Lateral Sclerosis patients.* BMC Genomics, 2009. **10**(1): p. 405.
41. Magrì, A., et al., *Hexokinase I N-terminal based peptide prevents the VDAC1-SOD1 G93A interaction and re-establishes ALS cell viability.* Scientific reports, 2016. **6**: p. 34802-34802.
42. Stankiewicz, T.R., et al., *Dysregulation of Rac or Rho elicits death of motor neurons and activation of these GTPases is altered in the G93A mutant hSOD1 mouse model of amyotrophic lateral sclerosis.* Neurobiology of Disease, 2020. **136**: p. 104743.

43. Boeynaems, S., et al., *Phase Separation of C9orf72 Dipeptide Repeats Perturbs Stress Granule Dynamics.* Mol Cell, 2017. **65**(6): p. 1044-1055.e5.
44. Hartmann, H., et al., *Proteomics and C9orf72 neuropathology identify ribosomes as poly-GR/PR interactors driving toxicity.* Life Sci Alliance, 2018. **1**(2): p. e201800070.
45. Bernardini, C., et al., *Mitochondrial network genes in the skeletal muscle of amyotrophic lateral sclerosis patients.* PLoS One, 2013. **8**(2): p. e57739.
46. Iridoy, M.O., et al., *Neuroanatomical Quantitative Proteomics Reveals Common Pathogenic Biological Routes between Amyotrophic Lateral Sclerosis (ALS) and Frontotemporal Dementia (FTD).* International journal of molecular sciences, 2018. **20**(1): p. 4.
47. Vonk, L.A., et al., *Mesenchymal Stromal/stem Cell-derived Extracellular Vesicles Promote Human Cartilage Regeneration In Vitro.* Theranostics, 2018. **8**(4): p. 906-920.
48. Nahm, M., et al., *ANXA11 mutations in ALS cause dysregulation of calcium homeostasis and stress granule dynamics.* Sci Transl Med, 2020. **12**(566).
49. Howells, J., et al., *In vivo evidence for reduced ion channel expression in motor axons of patients with amyotrophic lateral sclerosis.* J Physiol, 2018. **596**(22): p. 5379-5396.
50. Prudencio, M., et al., *Distinct brain transcriptome profiles in C9orf72-associated and sporadic ALS.* Nat Neurosci, 2015. **18**(8): p. 1175-82.
51. Dafinca, R., et al., *C9orf72 Hexanucleotide Expansions Are Associated with Altered Endoplasmic Reticulum Calcium Homeostasis and Stress Granule Formation in Induced Pluripotent Stem Cell-Derived Neurons from Patients with Amyotrophic Lateral Sclerosis and Frontotemporal Dementia.* Stem Cells, 2016. **34**(8): p. 2063-78.
52. Cohen, T.J., et al., *An acetylation switch controls TDP-43 function and aggregation propensity.* Nat Commun, 2015. **6**: p. 5845.
53. Oberstadt, M., et al., *TDP-43 and Cytoskeletal Proteins in ALS.* Mol Neurobiol, 2018. **55**(4): p. 3143-3151.
54. Vleminckx, V., et al., *Upregulation of HSP27 in a transgenic model of ALS.* J Neuropathol Exp Neurol, 2002. **61**(11): p. 968-74.
55. Wang, J., et al., *Copper-binding-site-null SOD1 causes ALS in transgenic mice: aggregates of non-native SOD1 delineate a common feature.* Hum Mol Genet, 2003. **12**(21): p. 2753-64.
56. Wang, J., et al., *Somatodendritic accumulation of misfolded SOD1-L126Z in motor neurons mediates degeneration: alphaB-crystallin modulates aggregation.* Hum Mol Genet, 2005. **14**(16): p. 2335-47.
57. Tummala, H., et al., *Inhibition of chaperone activity is a shared property of several Cu,Zn-superoxide dismutase mutants that cause amyotrophic lateral sclerosis.* J Biol Chem, 2005. **280**(18): p. 17725-31.
58. Seminary, E.R., S.L. Sison, and A.D. Ebert, *Modeling Protein Aggregation and the Heat Shock Response in ALS iPSC-Derived Motor Neurons.* Frontiers in Neuroscience, 2018. **12**.
59. Teyssou, E., et al., *Genetic analysis of SS18L1 in French amyotrophic lateral sclerosis.* Neurobiology of Aging, 2014. **35**(5): p. 1213.e9-1213.e12.
60. Aizawa, H., et al., *Dendrite development regulated by CREST, a calcium-regulated transcriptional activator.* Science, 2004. **303**(5655): p. 197-202.
61. Taylor, J.P., R.H. Brown, Jr., and D.W. Cleveland, *Decoding ALS: from genes to mechanism.* Nature, 2016. **539**(7628): p. 197-206.
62. Sasaki, S., *Autophagy in Spinal Cord Motor Neurons in Sporadic Amyotrophic Lateral Sclerosis.* Journal of Neuropathology & Experimental Neurology, 2011. **70**(5): p. 349-359.
63. Li, L., X. Zhang, and W. Le, *Altered macroautophagy in the spinal cord of SOD1 mutant mice.* Autophagy, 2008. **4**(3): p. 290-293.

64. Sellier, C., et al., *Loss of C9ORF72 impairs autophagy and synergizes with polyQ Ataxin-2 to induce motor neuron dysfunction and cell death.* Embo j, 2016. **35**(12): p. 1276-97.
65. Sullivan, P.M., et al., *The ALS/FTLD associated protein C9orf72 associates with SMCR8 and WDR41 to regulate the autophagy-lysosome pathway.* Acta Neuropathol Commun, 2016. **4**(1): p. 51.
66. Shi, Y., et al., *Haploinsufficiency leads to neurodegeneration in C9ORF72 ALS/FTD human induced motor neurons.* Nat Med, 2018. **24**(3): p. 313-325.
67. Madill, M., et al., *Amyotrophic lateral sclerosis patient iPSC-derived astrocytes impair autophagy via non-cell autonomous mechanisms.* Molecular Brain, 2017. **10**(1): p. 22.
68. Marrone, L., et al., *Isogenic FUS-eGFP iPSC Reporter Lines Enable Quantification of FUS Stress Granule Pathology that Is Rescued by Drugs Inducing Autophagy.* Stem Cell Reports, 2018. **10**(2): p. 375-389.
69. Bose, J.K., C.C. Huang, and C.K. Shen, *Regulation of autophagy by neuropathological protein TDP-43.* J Biol Chem, 2011. **286**(52): p. 44441-8.
70. Lee, M., et al., *Adipose-derived stem cell exosomes alleviate pathology of amyotrophic lateral sclerosis in vitro.* Biochem Biophys Res Commun, 2016. **479**(3): p. 434-439.
71. Chen, H.X., et al., *Exosomes derived from mesenchymal stem cells repair a Parkinson's disease model by inducing autophagy.* Cell Death Dis, 2020. **11**(4): p. 288.
72. Higelin, J., et al., *FUS Mislocalization and Vulnerability to DNA Damage in ALS Patients Derived hiPSCs and Aging Motoneurons.* Front Cell Neurosci, 2016. **10**: p. 290.
73. Dafinca, R., et al., *Impairment of Mitochondrial Calcium Buffering Links Mutations in C9ORF72 and TARDBP in iPS-Derived Motor Neurons from Patients with ALS/FTD.* Stem Cell Reports, 2020. **14**(5): p. 892-908.
74. Meng, F.G., et al., *Chondrogenesis of mesenchymal stem cells in a novel hyaluronate-collagen-tricalcium phosphate scaffolds for knee repair.* Eur Cell Mater, 2016. **31**: p. 79-94.
75. Prins, H.J., et al., *Bone-forming capacity of mesenchymal stromal cells when cultured in the presence of human platelet lysate as substitute for fetal bovine serum.* Tissue Eng Part A, 2009. **15**(12): p. 3741-51.
76. Théry, C., et al., *Isolation and characterization of exosomes from cell culture supernatants and biological fluids.* Curr Protoc Cell Biol, 2006. **Chapter 3**: p. Unit 3.22.
77. Melief, J., et al., *Characterizing primary human microglia: A comparative study with myeloid subsets and culture models.* Glia, 2016. **64**(11): p. 1857-68.

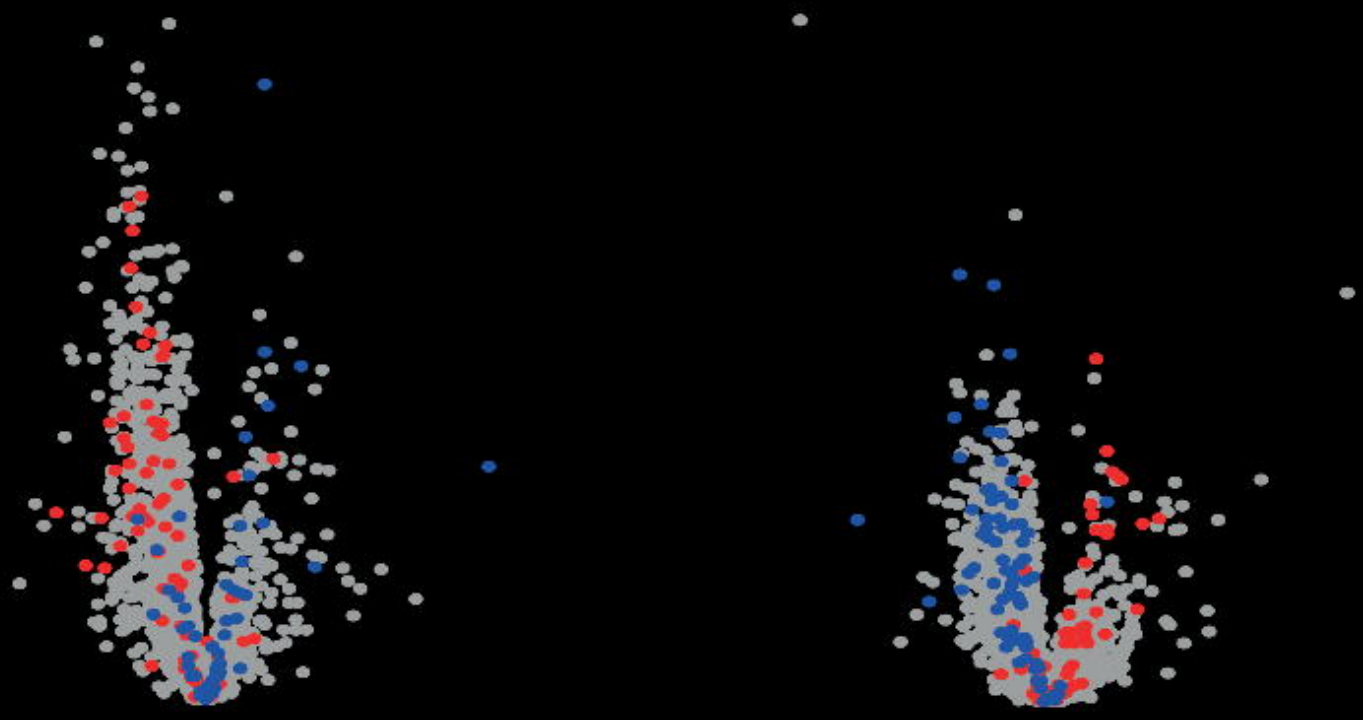

2.61	-3.83
2.26	-2.42
1.96	-1.53
1.70	-1.93
1.69	-2.29
1.56	-2.07
1.53	-1.06
1.49	-2.00
1.48	-1.74
1.43	-1.95
-1.52	1.07
-1.59	-0.54
-1.61	0.26
-1.61	-0.11
-1.63	1.07
-1.67	2.82
-1.81	0.37
-1.83	0.32
-1.88	-1.08
-8.28	7.28

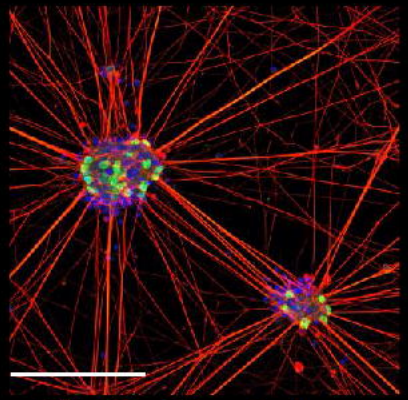

ISL1/TuJ/Hoechst

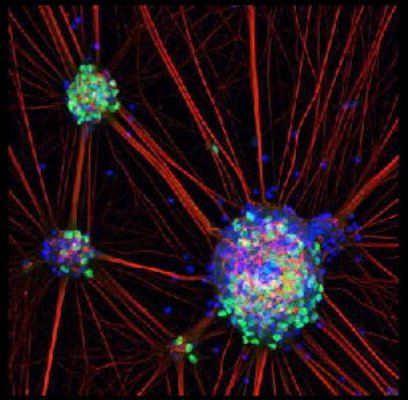

HB9/TuJ/Hoechst

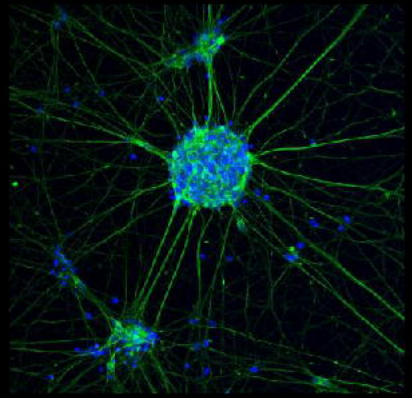

CHAT/ Hoechst

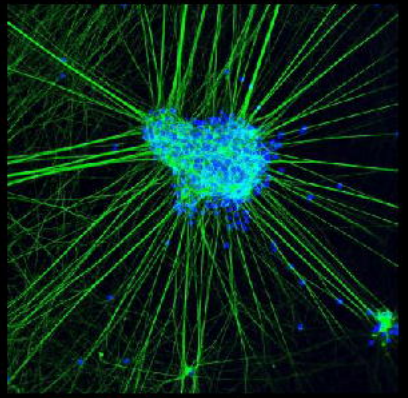

SMI32/ Hoechst

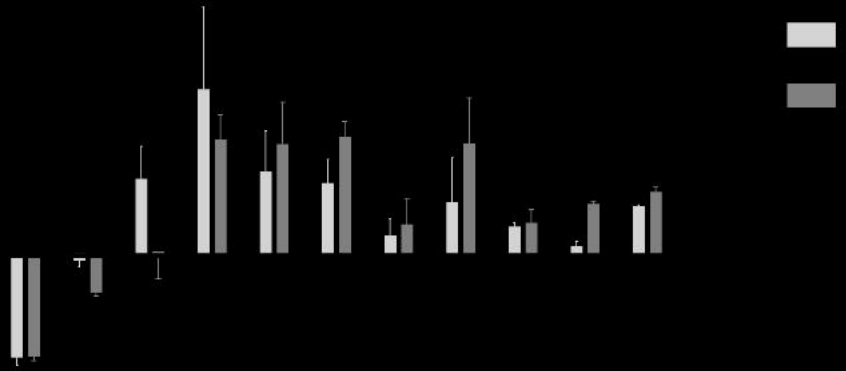

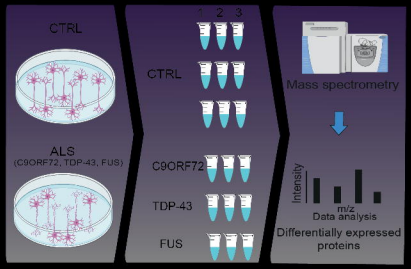

5.17		
4.29	0.11	0.36
2.88	6.13	
2.73	0.12	-1.52
2.33	-2.03	
2.31	1.20	
2.01	-0.10	
1.84		
1.80		
1.79	-1.06	
-5.99	4.21	-0.24
-2.30		0.96
-2.14	0.00	-0.66
-2.12	1.06	
-1.81	1.22	0.29
-1.73	-1.31	0.16
-1.69	1.31	0.03
-1.68	-1.24	-1.27
-1.67	1.17	-1.92
-1.65	0.24	-0.28
	6.83	
0.55	6.72	-0.73
-0.94	3.15	-1.00
0.66	3.14	
1.38	3.12	2.05
0.95	2.95	-0.89
0.13	2.61	-3.16
-0.26	2.57	-1.92
0.41	2.56	-0.28
0.54	2.55	-3.49
-0.16	-5.00	0.55
-0.51	-2.71	-0.78
0.72	-2.57	-0.44
	-2.49	0.53
1.44	-2.21	-6.94
0.80	-2.19	-4.83
-0.45	-2.09	-0.88
0.35	-2.06	
	-1.94	
0.81	-1.87	-2.78
-0.67	-0.10	9.65
-0.98		1.63
	-0.99	1.62
0.22	0.44	1.54
0.20	1.53	1.53
1.56	2.67	1.46
	-0.19	1.05
-2.30		0.96
-0.06		0.79
0.10	0.30	0.75
	-5.88	-11.12
0.95	0.60	-5.65
-0.16	1.53	-5.43
0.55	0.96	-5.41
0.89	0.25	-4.88
0.75	-0.43	-4.87
0.36	-0.47	-4.84
0.39	0.85	-4.83
0.68	0.84	-4.75
0.29	-0.20	-4.70

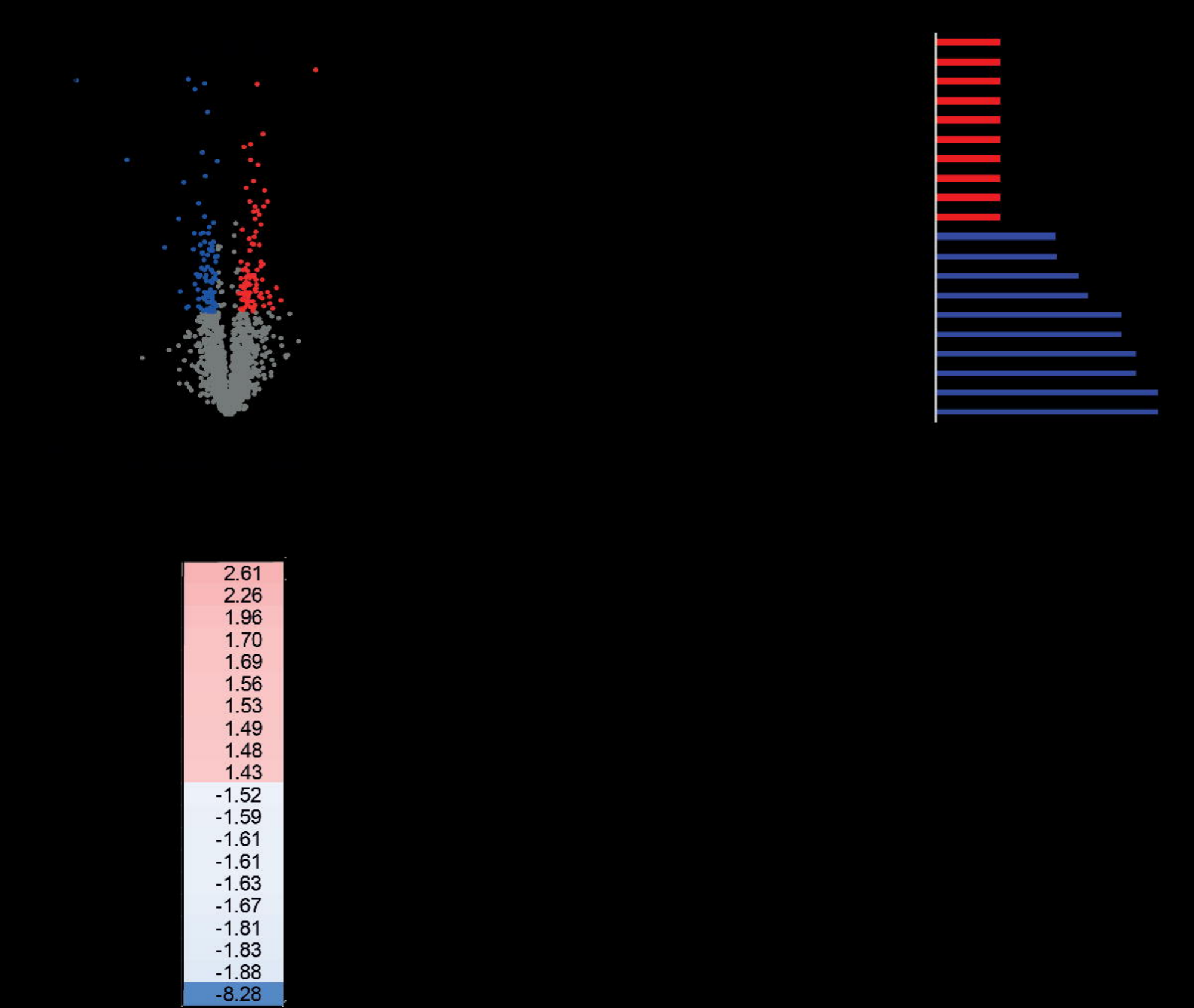
2.61
2.26
1.96
1.70
1.69
1.56
1.53
1.49
1.48
1.43
-1.52
-1.59
-1.61
-1.61
-1.63
-1.67
-1.81
-1.83
-1.88
-8.28

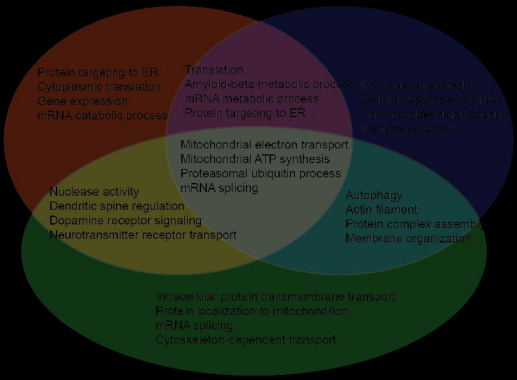

-3,251
-3,806
-2,823
-1,268
-2,645
-1,050
-3,227
-3,196
-0,609
-1,296
-2,554
-2,381
-4,753
-0,770
-2,131

-0,818
1,144
0,946
0,818

1,147
-1,832
-0,766
0,952
1,519

-1,250	-2,057
1,453	-3,796
1,829	-1,643

-0,894	-1,023
-0,782	-1,130
-2,296	0,981
-0,983	1,629
0,720	-3,820
0,876	-4,236
0,721	-2,640
0,601	-3,473
1,050	-2,627
0,793	-1,174

0,951	2,951
0,660	2,530

-1,677	-1,235	-1,267
0,970	3,728	1,367

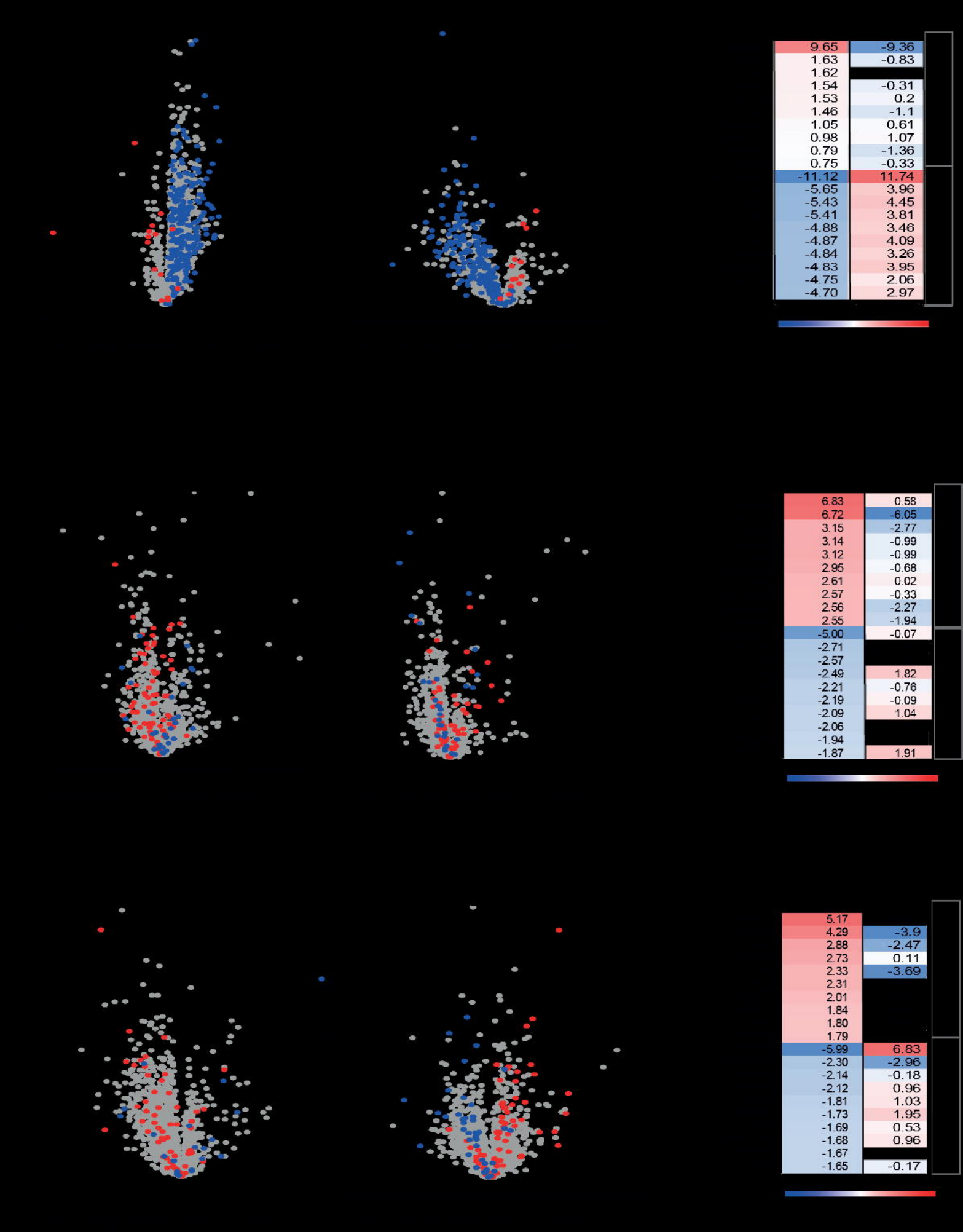
9.65 -9.36
1.63 -0.83
1.62
1.54 -0.31
1.53 0.2
1.46 -1.1
1.05 0.61
0.98 1.07
0.79 -1.36
0.75 -0.33
-11.12 11.74
-5.65 3.96
-5.43 4.45
-5.41 3.81
-4.88 3.46
-4.87 4.09
-4.84 3.26
-4.83 3.95
-4.75 2.06
-4.70 2.97
6.83 0.58
6.72 -6.05
3.15 -2.77
3.14 -0.99
3.12 -0.99
2.95 -0.68
2.61 0.02
2.57 -0.33
2.56 -2.27
2.55 -1.94
-5.00 -0.07
-2.71
-2.57
-2.49 1.82
-2.21 -0.76
-2.19 -0.09
-2.09 1.04
-2.06
-1.94
-1.87 1.91
5.17
4.29 -3.9
2.88 -2.47
2.73 0.11
2.33 -3.69
2.31
2.01
1.84
1.80
1.79
-5.99 6.83
-2.30 -2.96
-2.14 -0.18
-2.12 0.96
-1.81 1.03
-1.73 1.95
-1.69 0.53
-1.68 0.96
-1.67
-1.65 -0.17